A Study of Generalized Vortex Flow and Heat Transfer Involving Nanofluids

by

Sahreen Tahira

A thesis submitted in partial fulfilment of the requirements for the degree of Master of Science in Mathematics

Supervised by

Dr. Meraj Mustafa Hashmi

Department of Mathematics, School of Natural Sciences, National University of Sciences and Technology, Islamabad, Pakistan

FORM TH-4

National University of Sciences & Technology

MASTER'S THESIS WORK

We hereby recommend that the dissertation prepared under our supervision by: Ms. Sahreen Tahira, Regn No. 00000278416 Titled: A Study of Generalized Vortex Flow and Heat Transfer Involving Nanofluids be accepted in partial fulfillment of the requirements for the award of **MS** degree.

Examination Committee Members

1. Name: Dr. Mujeeb ur Rehman Signature:

2. Name: Dr. Muhammad Asif Farooq Signature:

External Examiner: Prof. Muhammad Ramzan Signature:

Supervisor's Name: Dr. Meraj Mustafa Hashmi Signature:

Head of Department

11/01/2021
Date

COUNTERSINGED

Date: 11/01/2021

Dean/Principal

This thesis is dedicated to my loving parents and to my siblings

for their prayers and lot of support

Table of Contents

Acknowledgments

Praise is to Almighty Allah, WHO is Creator of the world, the Answerer of prayers and the Source of peace, whose blessing and exaltation flourished to the sacred wealth of knowledge. Special praises and regards for His Last Messenger, Holy Prophet Hazrat Muhammad (صَلَّى ٱللَّٰهُ عَلَيْهِ وَآلِهِ وَسَلَّمَ)). Holy Prophet(صَلَّى ٱللَّٰهُ عَلَيْهِ وَآلِهِ وَسَلَّمَ)) said that I Am the light, whoever follows ME, will never be in the darkness.

I feel great pleasure in expressing my profound and heartiest gratitude to my respected supervisor Dr. Meraj Mustafa Hashmi, for his indispensable guidance, affection and active co-operation that made possible this work to meet its end successfully. work. May Allah shower his countless blessing upon them and bless him with good health and knowledge. I would like to pay my gratitude to my GEC members Dr. Mujeeb Ur Rehman and Dr. M. Asif Farooq, for their support and guidance in completing this thesis.

I owe my respect and gratitude to my family who has been a continuous source of motivation all along and has allowed me to encroach upon their love and patience. Words of thanks, surely insufficient and incomplete, are also cited for all my worthy teachers by whom I got my spiritual values and basis of education. Along with these staff members I would like to thank Dr. Ammar Mushtaq for his guidance and co-operation in my research work. I am also thankful to my friend Mamuna Azhar for her moral support. Finally, thanks to all my class fellows for their prayers and co-ordination.

Sahreen Tahira

List of Figures

List of Tables

Abstract

In this thesis, a nanofluid boundary layer that develops above a plane permeable surface is analysed numerically. The focus of this thesis is twofold. Firstly, to investigate the generalized vortex flow in a $Cu - Al_2O_3$/water-based hybrid nanofluid subjected to viscous dissipation effects using Tiwari and Das model. Secondly, to examine a two-phase Buongiorno mathematical model for a generalized vortex flow. In present work, vortex motion is characterized by a prescribed tangential flow with velocity proportional to r^m, where r is radial coordinate and m denotes the power-law index. Simulations are made by assuming a power-law surface temperature distribution. Different from previously adopted practice, the diffusion coefficients are not assumed constant here. A similarity solution is proposed, which transforms the constitutive equations into a coupled differential system whose solution is evaluated numerically by MATLAB function bvp4c. Results display a considerable expansion in thermal boundary layer whenever nanoparticles are present. Important quantities like normalized wall shear, disk cooling rate and entrained flow are scrutinized for varying choices of parameters. The contribution of Brownian diffusion and Soret effect on the vortex induced motion is studied. The graphical and tabular results demonstrate that these parameters provide a remarkable enhancement in the heat and mass transfer rate.

Chapter 1

Introduction

1.1 Basic Definitions and Concepts

Here are some basis definitions and concepts which are widely used in fluid dynamics.

1.1.1 Compressible vs Incompressible Flows

An incompressible fluid flow is the one in which density variations are negligible. All liquids are treated as incompressible fluids. On contrary, the fluid flows that are characterized by a varying density are said to be compressible. Most commonly encountered gases are compressible fluids. Continuity equations for compressible and incompressible flows are respectively:

$$\frac{\partial \rho}{\partial t} + \nabla.(\rho \mathbf{V}) = 0, \tag{1.1}$$

and

$$\nabla.\mathbf{V} = 0. \tag{1.2}$$

1.1.2 Ideal vs Real Flows

Ideal flows are the incompressible and irrotational fluid flows. In such fluids, shearing force between the fluid and the bounding surface is absent. On the other hand, fluid flows involving viscosity or surface shearing forces are termed as real flows.

1.1.3 Steady vs Unsteady Flows

In steady flows, all the physical quantities (such as density, velocity, acceleration etc) do not vary with time. Mathematically, for any quantity χ, one has:

$$\frac{\partial \chi}{\partial t} = 0, \tag{1.3}$$

For unsteady flow, the physical quantities exhibit time dependency. Therefore,

$$\frac{\partial \chi}{\partial t} \neq 0, \tag{1.4}$$

where χ is any physical quantity.

1.1.4 Laminar vs Turbulent Flows

Laminar flow is a kind of flow in which each fluid particle follows a definite path and streamlines do not cross each other. Turbulent flow, on the other hand, do not exhibit a regular

pattern of flow that leads to the rapid changes in physical properties of the fluid. For example, the flows in a pipe at low speed and flow of water along the edges of river/lake, falls in laminar flows. When a dye drop is injected in water, it spreads in all possible directions without following any proper pattern, thereby making the flow turbulent.

Reynolds number determines whether the flow is turbulent/laminar. It is laminar ($Re < 2000$) and turbulent for ($Re > 4000$). The laminar and turbulent regimes are shown in Fig. 1.1.

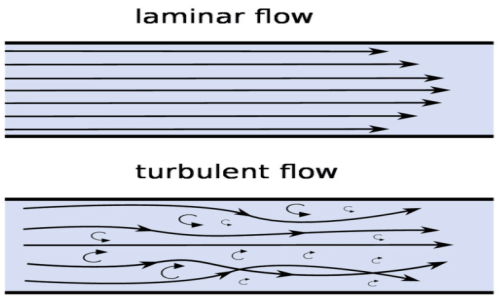

Fig. 1.1: Laminar and turbulent flow.

1.1.5 Nanofluid/Hybrid Nanofluid

A mixture of relatively small volume of nanometer sized solid substances such as nanoparticles, nanowires, nanotubes etc. suspended in liquids, is known as nanofluid. Nanoparticles are mainly oxides (Al_2O_3 , CuO, etc), metals (Au, Cu, Ag), carbides (SiC) and carbon tubules. For the very first time, the concept of adding the nanoparticles to the base fluid to increase the heat transfer rate in fluids was discovered by Masuda et al. [1]. These new generation fluids have been required by some industries to ensure quick and effective heat transfer coefficient for a variety of applications. These include automotive applications, nuclear reactor cooling, geothermal power extraction, smart fluids and many others. It has been detected that suspension of 0.3 vol% copper particles having diameter less than 10nm in ethylene glycol provides 40% improvement in thermal conductivity [2]. Some previously published reports (see, for instance, Ho et al. [3], Suresh et al. [4, 5] etc.) revealed marked improvement in thermal conductivity of water by dispersing small concentration of $Cu - Al_2O_3$ nanoparticles.

Hybrid nanofluids are novel class of working fluids produced by dispersing two or three small sized solid nanoparticles in conventional fluids (such as water, ethylene glycol, kerosene, vegetable oil etc.). Key factors affecting the thermal attributes of a hybrid nanofluid includes volume fraction, size and shape of nanoparticles used and mixing ratio of the two nanoparticles

[6, 7]. Devi and Devi [8] attempted the traditional stretching sheet induced flow through a water-based hybrid nanofluid and noticed a marked improvement in cooling rate of the sheet. Hybrid nanofluids perform effectively as compared to nanofluids. Waini et al. [9] found dual solutions for flow occurring over a permeable shrinking surface utilizing hybrid nanofluid. They also witnessed heat transfer enhancement for increasing solid volume fraction. Sheikholeslami [10] considered fluid flow inside a porous cavity filled with hybrid nanofluid, by including the aspects of shape factor and Brownian diffusion. Recently various contributions concerning hybrid nanofluid analysis for boundary layer flows are conducted (see, for example, [11-15]).

1.2 Boundary Layer Flows

A thin layer surrounding the boundary, in which the viscosity effects are significant and important in determining the fluid flow, is known as boundary layer. It acts as a buffer region between the wall and the free stream region. All these flows that follow the boundary layer theory (proposed by Prandlt in 1904) are termed as boundary layer flows. Fig. 1.2 represents velocity boundary layer thickness over a flat plate at zero incidence.

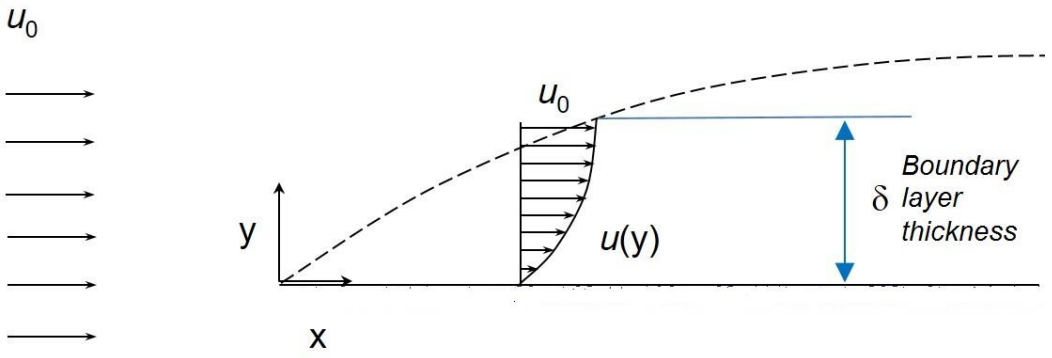

Fig. 1.2: Boundary layer thickness in laminar flow.

Some of the special boundary layer flows are described below that follows the boundary layer theory.

1.2.1 Von Kármán Flow

Von Kármán [55] pointed out a flow situation where an infinite disk lying in the plane $z = 0$ revolves in its own plane about the vertical axis with constant angular velocity ω. The disk is placed in an incompressible Newtonian fluid of viscosity μ and density ρ. The lack of centrifugal force near the surface induces a radially outward motion which in turn leads to a

downward vertical motion. Rotational effects and hence radial pressure gradient $(\partial p/\partial r)$ is expected to vanish as $z \to \infty$. The rotational axisymmetric condition leads us to ignore the change in azimuthal ϕ-direction. The above problem is translated into the following equations:

$$u\frac{\partial u}{\partial r} + w\frac{\partial u}{\partial z} - \frac{v^2}{r} = -\frac{1}{\rho}\frac{\partial p}{\partial r} + \nu(\nabla^2 u - \frac{u}{r^2}), \tag{1.5}$$

$$u\frac{\partial v}{\partial r} + w\frac{\partial v}{\partial z} + \frac{uv}{r} = \nu\left(\nabla^2 v - \frac{v}{r^2}\right), \tag{1.6}$$

$$u\frac{\partial w}{\partial r} + w\frac{\partial w}{\partial z} = -\frac{1}{\rho}\frac{\partial p}{\partial z} + \nu\nabla^2 w. \tag{1.7}$$

The problem is subjected to the required boundary conditions:

$$\begin{aligned} u = 0,\ v = r\omega,\ w = 0,\ T = T_w \quad &\text{at} \quad z = 0, \\ u \to 0,\ v \to 0,\ T \to T_\infty \quad &\text{as} \quad z \to \infty. \end{aligned} \tag{1.8}$$

Von Kármán [55] showed that the governing Eqs. (1.5) – (1.7) are reduceable into ODEs by following transformations:

$$\begin{aligned} u = r\omega F(\eta),\ v = r\omega G(\eta),\ w = \sqrt{\nu\omega}H(\eta), \\ p = 2\mu_f \omega p(\eta) + p_\infty \quad \text{with } \eta = \sqrt{\frac{\omega}{\nu}}z. \end{aligned} \tag{1.9}$$

Eqs (1.5) – (1.8) will convert into the following system via (1.9):

$$H' + 2F = 0, \tag{1.10}$$

$$F'' - HF' - F^2 + G^2 = 0, \tag{1.11}$$

$$G'' - HG' + 2FG = 0. \tag{1.12}$$

$$\begin{aligned} F = 0,\ G = 1,\ H = 0 \quad &\text{at} \quad \eta = 0, \\ F \to 0,\ G \to 0 \ \text{as} \quad &\eta \to \infty. \end{aligned} \tag{1.13}$$

The functions F, G and H obtained from Eqs. (1.10) – (1.12) are shown graphically in Fig 1.3.

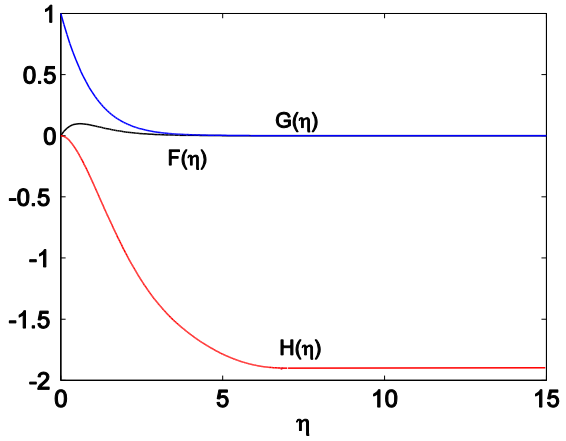

Fig. 1.3: Velocity profiles for Von Kármán flow.

1.2.2 Bödewadt Flow

Bödewadt flow [17] is a rotationally symmetric flow that occurs over a stationary disk such that the fluid at far field is in a state of rigid body rotation about the vertical axis. Centrifugal force is greatly decreased near the surface due to which a radial inflow is developed that ultimately triggers an axially upward motion. Fluid motion will be governed by the same equations (1.5) – (1.7). Boundary conditions in this case are given below.

$$\begin{aligned} u = 0,\ v = 0,\ w = 0 \quad &\text{at} \quad z = 0, \\ u \to 0,\ v = r\omega \quad &\text{as} \quad z \to \infty. \end{aligned} \tag{1.14}$$

At far-field, radial pressure gradient equals to centrifugal force is imposed, so we have $\partial p/\partial r = \rho r^2 \omega^2$. With transformations (1.9), the following system is obtained:

$$H' + 2F = 0, \tag{1.15}$$

$$F'' - HF' - F^2 + G^2 - 1 = 0, \tag{1.16}$$

$$G'' - HG' + 2FG = 0. \tag{1.17}$$

$$\begin{aligned} F = 0,\ G = 0,\ H = 0 \quad &\text{at} \quad \eta = 0, \\ F \to 0,\ G \to 1 \quad &\text{as} \quad \eta \to \infty. \end{aligned} \tag{1.18}$$

The velocity profiles of above governing Eqs. (1.15) – (1.17) are shown in Fig. 1.4.

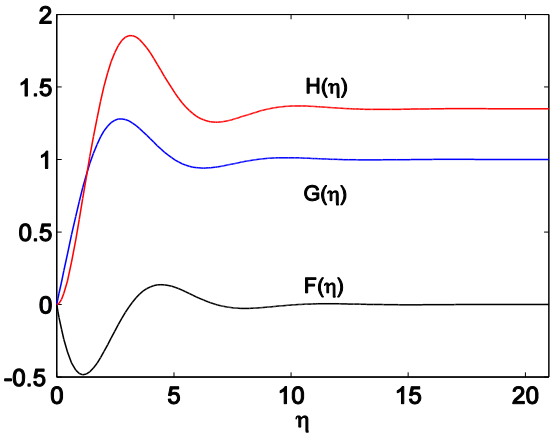

Fig. 1.4: Velocity profiles of Bödewadt flow.

1.2.3 Vortex Flow

For this kind of rotationally symmetric motion, the tangential velocity is assumed to satisfy a power law form, that is $v \sim r^m$, where r is radial co-ordinate and m is power law index. There are two special cases of vortex flow i.e. potential vortex ($m = -1$) and rigid body rotation ($m = 1$). In potential vortex, also known as irrotational flow, there is an inverse relation between velocity of the fluid and distance r from the vortex axis. Whereas in rigid body rotation there is direct relation of velocity and distance r from the axis of rotation. Rahman and

Andersson generalized the vortex flow with the heat transfer in [56]. Boundary conditions for this flow are expressed as follows:

$$\begin{gathered} u = 0,\ \ v = 0,\ \ w = v_0\left(\frac{\nu}{v_0 r_0}\right)^{1/2}\left(\frac{r}{r_0}\right)^{n-1}(n+1),\ \ \text{at}\ \ z = 0, \\ u \to 0,\ \ v \to v_\infty = v_0\left(\frac{r}{r_0}\right)^{2n-1} \qquad \text{as} \quad z \to \infty. \end{gathered} \tag{1.19}$$

Using the similarity transformations:

$$\begin{gathered} u = -v_0\left(\frac{r}{r_0}\right)^{2n-1} F(\eta),\ \ v = v_0\left(\frac{r}{r_0}\right)^{2n-1} G(\eta), \\ w(r,z) = v_0\left(\frac{\nu_f}{v_0 r_0}\right)^{1/2}\left(\frac{r}{r_0}\right)^{n-1}\left[(n+1)H(\eta) + (n-1)\eta F(\eta)\right], \\ p = \frac{\rho_f {v_0}^2}{4n-2}\left(\frac{r}{r_0}\right)^{4n-2} \quad \text{with} \quad \eta = \left(\frac{z}{r_0}\right)\left(\frac{r}{r_0}\right)^{n-1}\left(\frac{v_0 r_0}{\nu_f}\right)^{1/2}. \end{gathered} \tag{1.20}$$

The governing Eqs. (1.5) – (1.7) are transformed into the following ODE's:

$$H' - F = 0, \tag{1.21}$$

$$F'' - (n+1)HF' - F^2 - G^2 + 1 = 0, \tag{1.22}$$

$$G'' - (n+1)HG' + 2nFG = 0. \tag{1.23}$$

And the transformed boundary conditions are:

$$\begin{gathered} F = 0,\ \ G = 0,\ \ H = 1 \ \ \text{at} \ \ \eta = 0, \\ F \to 0,\ \ G \to 1 \quad \text{as} \quad \eta \to \infty. \end{gathered} \tag{1.24}$$

System (1.21) – (1.24) is solved numerically by MATLAB package bvp4c. Few results are shown in the Fig. 1.5 (a-c) are:

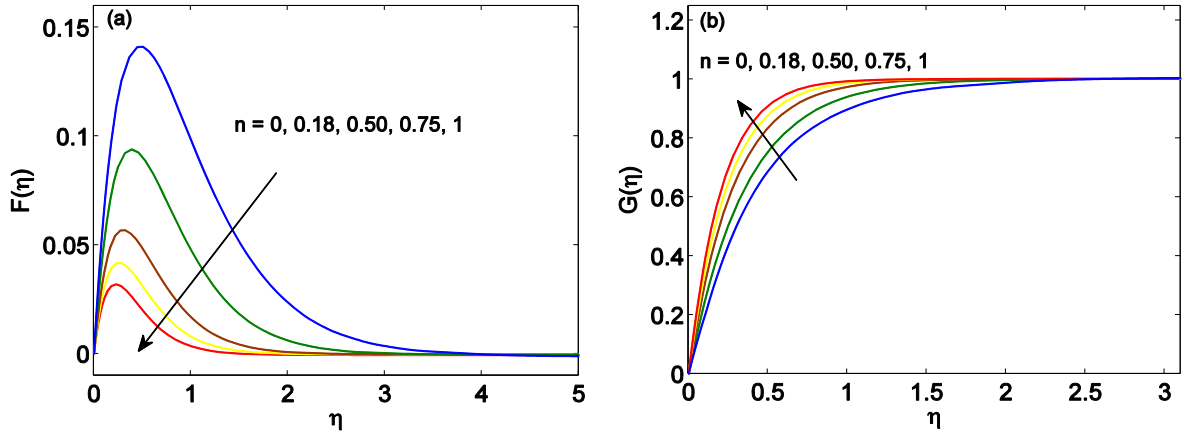

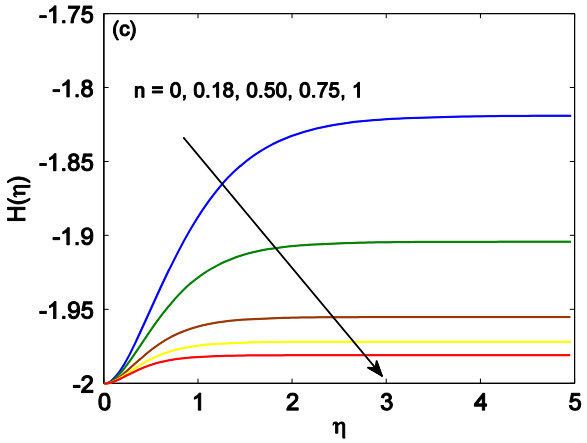

Fig. 1.5 (a-c): Velocity profiles for different values of n in a generalized vortex flow.

1.3 Mathematical Models for Thermal Transport Using Nanofluids

1.3.1 Tiwari and Das Model

The continuity, momentum and energy equations in this model are:

$$\nabla.\mathbf{V} = 0, \tag{1.25}$$

$$\rho_{nf}\left\{\frac{\partial \mathbf{V}}{\partial t} + (\mathbf{V}.\nabla)\mathbf{V}\right\} = -\nabla p + \mu_{nf}\nabla^2\mathbf{V}, \tag{1.26}$$

$$\left(\rho C_p\right)_{nf}(\mathbf{V}.\nabla)T = k_{nf}\,\nabla^2 T. \tag{1.27}$$

where $\rho_{nf}, \mu_{nf}, \left(\rho C_p\right)_{nf}$ and k_{nf} are effective density, effective dynamic viscosity, effective specific heat capacity and effective thermal conductivity of nanofluids respectively. Mathematical expressions of such quantities are given in table 1.1.

Table 1.1: Effective thermophysical properties of nanoparticles with subscripts f, nf and s_1 and s_2 representing fluid, nanofluid and solid phases (particles) respectively [34].

Properties	Models
Dynamic viscosity (μ_{nf})	$\mu_{nf} = \mu_f(1-\phi)^{-2.5}$
Density (ρ_{nf})	$\rho_{nf} = (1-\phi)\rho_f + \phi\rho_s$
Heat capacity $\left(\rho C_p\right)_{nf}$	$\left(\rho C_p\right)_{nf} = (1-\phi)(\rho C_p)_f + \phi(\rho C_p)_s$
Thermal conductivity (k_{nf})	$k_{nf} = k_f \dfrac{k_s + 2k_f - 2\phi(k_f - k_s)}{k_s + 2k_f + \phi(k_f - k_s)}$

1.3.2 Buongiorno Model

Buongiorno [16] considered incompressible nanofluid flow with the two key effects namely Brownian motion and thermophoresis. For this model, continuity and momentum equations are of the forms:

$$(\nabla.\mathbf{V}) = 0, \tag{1.28}$$

$$\rho_{nf}\left\{\frac{\partial \mathbf{V}}{\partial t} + (\mathbf{V}.\nabla)\mathbf{V}\right\} = -\nabla p - \nabla.\boldsymbol{\tau}. \tag{1.29}$$

where $\mathbf{V}$ is velocity vector, ρ_{nf} is density of nanoparticles and $\boldsymbol{\tau}$ is stress tensor. Energy equation without viscous dissipation term is considered as:

$$(\rho C_p)_{nf}\left(\frac{\partial T}{\partial t} + (\mathbf{V}.\nabla)T\right) = \nabla.\mathbf{q} - C_p\mathbf{J_p}.\nabla T, \tag{1.30}$$

where $\left(\rho C_p\right)_{nf}$ is specific heat capacity, $\mathbf{q}$ is heat flux and $\mathbf{J_p}$ is nanoparticle mass flux and T is the local temperature of the nanofluid. The mass flux $\mathbf{J_p}$, due to Brownian diffusion and thermophoresis are considered as:

$$\mathbf{J_p} = -\rho_p\left(D_B\nabla\phi + \frac{D_T\nabla T}{T}\right), \tag{1.31}$$

in which D_B and D_T are Brownian and thermophoretic diffusion coefficients. These are further expressed as $C_T = D_B/T$ and $C_T = D_T/\phi$,where ϕ is nanoparticle volume fraction. Energy equation (1.30) in view of (1.31) can be expressed as:

$$\left(\rho C_p\right)_{nf}\left(\frac{\partial T}{\partial t} + (\mathbf{V}.\nabla)T\right) = \nabla.\left(k_{nf}\nabla T\right) + C_p\rho_p\left(C_B T\nabla\phi + C_T\phi\frac{\nabla T}{T}\right).\nabla T. \tag{1.32}$$

Now the concentration equation is given by:

$$\begin{aligned}\left(\frac{\partial \phi}{\partial t} + (\mathbf{V}.\nabla)\phi\right) &= -\frac{1}{\rho_p}\nabla.\mathbf{J_p},\\ \left(\frac{\partial \phi}{\partial t} + (\mathbf{V}.\nabla)\phi\right) &= \nabla.\left(C_B T\nabla\phi + C_T\phi\frac{\nabla T}{T}\right).\end{aligned} \tag{1.33}$$

1.4 Some Dimensionless Parameters

Following are some well-known dimensionless parameters in fluid dynamics.

1.4.1 Reynolds Number

Reynolds number is the ratio of inertial force to the viscous force. It allows us to differentiate whether the flow is laminar or turbulent. At low Re we have laminar regime (i.e. $Re < 2000$) and for high Reynolds number ($Re > 4000$) we have turbulent regime. Mathematically,

$$Re = \frac{vL}{\nu}, \tag{1.34}$$

where v is velocity of the fluid, L is characteristic length and ν is kinematic viscosity of fluid.

1.4.2 Prandlt Number

It is a dimensionless number that gives the ratio of kinematic viscosity to thermal diffusivity. Mathematically it is defined as:

$$Pr = \frac{\nu}{\alpha}, \tag{1.35}$$

where ν is the kinematic viscosity and α is thermal diffusivity that is further is defined as $\alpha = k/\rho C_P$ in which k represents thermal conductivity, ρ denotes density and C_p shows specific heat capacity at constant pressure.

1.4.3 Eckert Number

It is a dimensionless number that defines the ratio of kinetic energy of the fluid to the enthalpy difference. It is commonly used to describe the convective heat transfer in fluid flows. Mathematically it is defined as:

$$Ec = \frac{v^2}{C_p \Delta T}, \tag{1.36}$$

where v is the fluid velocity and ΔT shows the temperature difference between wall and far-field temperature.

1.4.4 Nusselt Number

It appears when there is a heat transfer from convection flow to conduction flow in fluids across the boundary. The heat transfer is perpendicular to surface of the boundary. Mathematically,

$$Nu = \frac{QL}{k}, \tag{1.37}$$

where Q is convective heat transfer coefficient, L is length of the disk/sheet and k is thermal conductivity of the fluid.

1.5 Literature Review

The problem representing steadily revolving flow above a plane stationary surface was resolved by Bödewadt [17] in 1940. After the theoretical work published by Bödewadt, Bödewadt's boundary layer was observed in rotor-stator system, as pointed out by Batchelor [18]. He investigated two parameter families of solutions representing rotationally symmetric flow. The first case deals with flow between two parallel disks such that one is stationary and the other revolves at a uniform angular velocity. The second scenario involves fluid motion over an infinite rotating plane through origin. The problem of rotating fluid infinite in extent above a rotating boundary, of which Bödewadt's work is a special case, was explored by Hannah [19]. Later, Nath and Venkatachala [20] revisited Bödewadt's analysis in the existence of suction and vertical magnetic field effects.

Therefore, mentioned initial papers led to the various novel research findings about the Bödewadt flow and resulting heat transfer. In a series of papers by Sahoo [21, 22], Bödewadt's boundary layer was explored under different situations using rheological equation of Reiner-Rivlin fluid model. A marked growth in boundary layer was visible whenever material fluid parameter signifying cross-viscosity effect was increased. It should be remarked here that Turkyilmazoglu [23] revisited the Bödewadt model when the stationary surface was allowed to stretch radially at a uniform rate. A comparison of different non-Newtonian models for Bödewadt flow was critically assessed by Griffiths [24]. Joshi et al. [25] made an effort to discuss Bödewadt flow of variable viscosity fluid. Similarity profiles shown in [25] do not preserve the asymptotic decay condition, which questions the validity of numerical method used. Rahman and Andersson [26] published an excellent article in which Bödewadt flow near a permeable boundary was studied numerically. The authors clearly demonstrated that physically acceptable solution of thermal energy equation in Bödewadt flow exists if direction of axial flow is turned downward. This was accomplished by imposing adequate amount of suction at the wall. Above outcomes are in contrast to the results shown by Sahoo [21] where temperature profiles are apparently realistic even when axial flow is directed upwards. It is believed that results of Sahoo [22] were obtained with an unnoticed sign error in the energy equation. Furthermore, the action of radial stretching can also reverse the direction of axial flow and can lead to realistic solution as noted in Turkyilmazoglu [23]. Motivated by Rahman and Andersson [26], we explored Bödewadt flow with different physical effects in our recent papers [27-29].

Another popular model which is widely implied by researchers is Buongiorno [16] that takes seven different physical effects that contribute to the thermal conductivity enhancement in nanofluids like inertia, magnus effect, diffusiophoresis, fluid drainage, gravity, Brownian motion and thermophoresis. He deduced that Brownian motion and thermophoresis effects are of great importance in the enhancement of heat transfer rate. Sheikoleslami et al [30] has work on unsteady flow between parallel plates using Buongiorno model and analysed the different parameters effects on the nanofluid. Steady MHD laminar flow on a shrinking rotating disk is studied by Turkiylmazoglu [31] under the influence of magnetic field. Domairry [32] concluded that, using Buongiorno nanofluid model, the increment in the volume fraction boundary layer and reduction in the thermal boundary layer as a result of natural convection. Arifin [33] has investigated the Buongiorno model under the influence of various parameter like suction, Brownian motion, thermophoresis, to study the heat transfer rate. Oztup [34] using

Rayleigh–Bénard problem examined the effects of Brownian motion and thermophoresis and he had deduced that there is a remarkable increase in heat transfer. Devi [35] has analyzed the model under the same parameters as of (Haddad [36], Wen [37] and many others [38-41]) for forced convective nanofluid with revised boundary conditions over a porous disk.

Sheremet [42] found the relationship between the heat transfer strength and the heater location/Rayleigh number taking Brownian motion and thermophoresis into account. Heat transfer is being investigated under the influence of heat flux by Nayak [43] and he observed that the mass transfer rate reduces as compare to the rate of heat transfer in non-linear convective Falkner flow. Sheremet [44] extrapolated that the addition of nanoparticles changes the flow type under different values of Rayleigh number. Brownian motion and thermophoretic effects on stretchable disk are examined by Khan [45] and inferred that the thermophoretic effect increases both the heat and mass transfer rate. Effects of different parameters like Brownian motion, thermophoresis, buoyancy ratio, Lewis number are interpreted by (see in [46-48]). They found that the dependency of Nusselt number and Sherwood number are in increasing trend with buoyancy ratio, Rayleigh number and thermophoretic effect and decreasing for Brownian motion and Lewis number. Rokni [49] did an investigation using Buongiorno model with different parameters for radiation and heat transfer rate and came to the conclusion that velocity and concentration profiles increases while the thermal boundary layer shrinks with the increase of melting parameters. Mahmoodi [50] examined the enhancement of heat transfer for kerosene-alumina and deduces that Nusselt number is decreasing function of Brownian and thermophoresis. The combined flow for Buongiorno model and Cattaneo-Christov heat and mass fluxes is examined by Khan [51]. He concluded that the for increment in thermophoresis enhances the heat and mass transfer rates whereas the increase in Brownian motion leads to the shrinking of the thermal and nanoparticle concentration boundary layer. Later on, Raizah [52] has explored the nanofluid inside the rough boundaries. Various temperature differences, roughness and Darcy effect has studied using the Buongiorno model by simple Algorithm. Xu [53] studies the flow between two-layer channel using Buongiorno model in the presence of electro-kinetic effect and deduced that the Brownian motion and other parameters alter the flow behaviour of nanofluids. The nanofluid is investigated in the presence of magnetic fields by Wakif [54] and stability is empowered by Rayleigh number and further depends on volume fraction and size of nanoparticles.

This thesis fills two gaps, firstly to formulate and analyse the generalized vortex flow and heat transfer over permeable surface embedded in a $Cu - Al_2O_3$/water-based hybrid nanofluid.

Secondly, we are interested to investigate Buongiorno mathematical model for generalized vortex flow without relying on usual assumptions of constant diffusion coefficient. In both the problems the power law surface temperature distribution is considered, which is essential for the governing equations to be self-similar, the collocation method-based MATLAB package bvp4c is utilized for the computational purposes to solve numerous parameters, like thermophoresis, suction Brownian motion and power law index and many more to see their effects on heat and mass transfer rate. In addition, the contribution of viscous dissipation term on the generalized vortex flow situation is assessed, which is yet to be explored.

Chapter 2

A Study of Generalized Vortex Flow on Hybrid Nanofluid over a Non-Isothermal Surface with Viscous Dissipation

2.1 Introduction

In this chapter, the generalized vortex for $Cu - Al_2O_3$/water-based hybrid nanofluid is investigated. It will be shown later that energy equation has a self-similar solution only when a quadratic temperature distribution is imposed. MATLAB package bvp4c is implemented to achieve numerical solutions for a wide range of controlling parameters. Subtle fluid dynamics concepts including wall drag coefficient and heat transfer rate are assessed in the existence of new physical mechanisms namely heat dissipation in this study.

2.2 Mathematical Modelling

We assume that a $Cu - Al_2O_3$/water hybrid nanofluid revolves steadily about the vertical axis, above a stationary permeable planar surface. Fluid rotation at far-field is characterized by power-law tangential velocity distribution $v \sim r^m$ with power $m = 2n - 1$ as prescribed parameter. The disk is placed in the plane $z = 0$ of the cylindrical coordinate system (r, φ, z) and (u, v, w) denotes the projections of velocity vector along $r-, \varphi-$ and $z-$ directions respectively. Different from [56], viscous dissipation effects are incorporated in the present model. Akin to the classical Bödewadt flow, the rotationally symmetry flow assumptions allow one to neglect derivatives in the $\varphi-$ direction. Applying boundary layer assumptions, vortex flow of nanofluid with the heat dissipation effects is governed by the following equations:

$$\frac{\partial}{\partial r}(ru) + \frac{\partial}{\partial z}(rw) = 0, \tag{2.1}$$

$$u\frac{\partial u}{\partial r} - \frac{v^2}{r} + w\frac{\partial u}{\partial z} = -\frac{1}{\rho_{hnf}}\frac{\partial p}{\partial r} + \nu_{hnf}\left(\frac{\partial^2 u}{\partial z^2}\right), \tag{2.2}$$

$$u\frac{\partial v}{\partial r} + \frac{uv}{r} + w\frac{\partial v}{\partial z} = \nu_{hnf}\left(\frac{\partial^2 v}{\partial z^2}\right), \tag{2.3}$$

$$(\rho C_p)_{hnf}\left(u\frac{\partial T}{\partial r} + w\frac{\partial T}{\partial z}\right) = k_{hnf}\frac{\partial^2 T}{\partial z^2} + \mu_{hnf}\left\{\left(\frac{\partial u}{\partial z}\right)^2 + \left(\frac{\partial v}{\partial z}\right)^2\right\}, \tag{2.4}$$

where ρ_{hnf}, ν_{hnf}, $(\rho C_p)_{hnf}$ and k_{hnf} denotes the effective density, kinematic viscosity, heat capacity and thermal conductivity of hybrid nanofluid respectively. Theoretical models of these

quantities are presented in Table 2.1 whereas thermophysical properties of water and nanoparticles are listed in Table 2.2.

Table 2.1: Effective thermophysical properties of hybrid nanofluids where subscripts f, nf, hnf and s_1 and s_2 correspond to fluid, nanofluid, hybrid nanofluid and solid phases (particles) respectively (Devi and Devi [8]).

Properties	Models
Dynamic viscosity (μ_{hnf})	$\mu_{hnf} = \mu_f(1-\phi_1)^{-2.5}(1-\phi_2)^{-2.5}$
Density (ρ_{hnf})	$\rho_{hnf} = (1-\phi_2)\left[(1-\phi_1)\rho_f + \phi_1\rho_{s1}\right] + \phi_2\rho_{s2}$
Heat capacity $(\rho C_p)_{hnf}$	$(\rho C_p)_{hnf} = (1-\phi_2)\{(1-\phi_1)(\rho C_p)_f + \phi_1(\rho C_p)_{s1}\} + \phi_2(\rho C_p)_{s2}$
Thermal conductivity(k_{hnf})	$k_{hnf} = k_{nf}\frac{k_{s2}+2k_{nf}-2\phi_2(k_{nf}-k_{s2})}{k_{s2}+2k_{nf}+\phi_2(k_{nf}-k_{s2})}$, $k_{nf} = k_f\frac{k_{s1}+2k_f-2\phi_1(k_f-k_{s1})}{k_{s1}+2k_f+\phi_1(k_f-k_{s1})}$

Table 2.2: Thermophysical properties of base fluids and nanoparticles (Oztop and Abu-Nada [34])

Property	Base fluid (H_2O)	Cu	Al_2O_3
C_p(J/kg)	4179	385	765
k(W/mK)	0.613	400	40
ρ(kg/m^3)	997.1	8933	3970

Following boundary conditions are considered for generalized vortex flow [56]:

$$u = 0,\ \ v = 0,\ \ w = Av_0\left(\frac{v_f}{v_0 r_0}\right)^{1/2}\left(\frac{r}{r_0}\right)^{n-1}(n+1),\ \ T = T_w(r)\ \text{ at }\ z = 0,$$
$$u \to 0,\ \ v \to v_\infty = v_0\left(\frac{r}{r_0}\right)^{2n-1},\ \ T \to T_\infty \quad \text{as} \quad z \to \infty. \tag{2.5}$$

The disc temperature T_w is assumed to vary in the radial direction according to $T_w(r) = T_\infty + T_0(r/r_0)^{2(2n-1)}$ and $A < 0$ is termed as wall suction parameter. It will be shown later that such dependency leads us to the self-similar governing system.

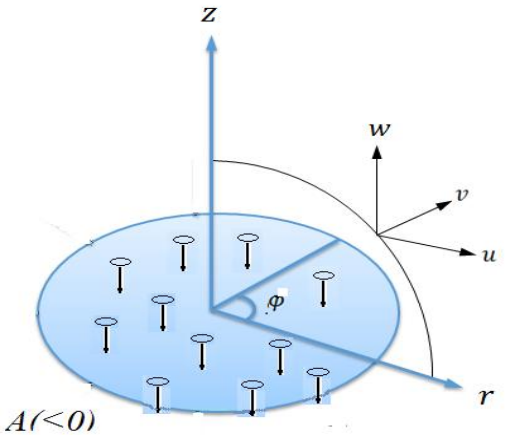

Fig. 2.1: Physical configuration and coordinate system.

We seek a similarity solution in the following forms [56]:

$$\begin{aligned} u(r,z) &= -v_0\left(\frac{r}{r_0}\right)^{2n-1} F(\eta), \\ v(r,z) &= v_0\left(\frac{r}{r_0}\right)^{2n-1} G(\eta), \\ w(r,z) &= v_0\left(\frac{\nu_f}{v_0 r_0}\right)^{1/2}\left(\frac{r}{r_0}\right)^{n-1} [(n+1)H(\eta) + (n-1)\eta F(\eta)], \\ p(r) &= \frac{\rho_{hnf}{v_0}^2}{4n-2}\left(\frac{r}{r_0}\right)^{4n-2}, \quad T(r,z) = T_\infty + (T_w - T_\infty)\theta(\eta), \end{aligned} \tag{2.6}$$

where η similarity variable is defined below:

$$\eta = \left(\frac{z}{r_0}\right)\left(\frac{r}{r_0}\right)^{n-1}\left(\frac{v_0 r_0}{\nu_f}\right)^{1/2}. \tag{2.7}$$

In the light of variables (2.6) governing equations (2.1) – (2.4) are transformed as follows:

$$H' - F = 0, \tag{2.8}$$

$$\frac{1}{\epsilon_1\epsilon_2}F'' - (n+1)HF' - (1-2n)F^2 - G^2 + 1 = 0, \tag{2.9}$$

$$\frac{1}{\epsilon_1\epsilon_2}G'' - (n+1)HG' + 2nFG = 0, \tag{2.10}$$

$$\frac{1}{\epsilon_3}\frac{k_{hnf}}{k_f}\theta'' - (n+1)PrH\theta' + 2(2n-1)Pr\,H'\theta + \frac{PrEc}{\epsilon_1\epsilon_3}\left(F'^2 + G'^2\right) = 0, \tag{2.11}$$

where,

$$\epsilon_1 = (1-\phi_1)^{2.5}(1-\phi_2)^{2.5}, \quad \epsilon_2 = (1-\phi_2)\{(1-\phi_1) + \phi_1\rho_{S1}/\rho_f\} + \phi_2\rho_{S2}/\rho_f,$$

$$\epsilon_3 = (1-\phi_2)\left\{(1-\phi_1) + \phi_1\left(\rho C_p\right)_{S1}/(\rho C_p)_f\right\} + \phi_2\left(\rho C_p\right)_{S2}/(\rho C_p)_f.$$

In Eqs. (2.8) – (2.11), $Pr = \left(\rho C_p\right)_f \nu_f/k_f$, represents base fluid Prandlt number and $Ec = v_\infty^2/\left(C_p\right)_f(T_w - T_\infty)$ defines the constant Eckert number.

The boundary conditions (2.5) transform to:

$$\begin{aligned} F = 0,\ G = 0,\ H = A,\ \theta = 1 \quad \text{at} \quad \eta = 0, \\ F \to 0,\ G \to 1,\ \theta \to 0 \quad \text{as} \quad \eta \to \infty. \end{aligned} \tag{2.12}$$

The radial and azimuthal shear stresses at the surface are evaluated as follows:

$$\tau_r = \mu_{hnf}\left(\frac{\partial u}{\partial z}\right)_{z=0} = -\frac{\mu_f}{(1-\phi_1)^{2.5}(1-\phi_2)^{2.5}}\left(\frac{v_0}{r_0}\right)\left(\frac{v_0 r_0}{\nu_f}\right)^{1/2}\left(\frac{r}{r_0}\right)^{3n-2} F'(0), \tag{2.13}$$

$$\tau_\phi = \mu_{hnf}\left(\frac{\partial v}{\partial z}\right)_{z=0} = \frac{\mu_f}{(1-\phi_1)^{2.5}(1-\phi_2)^{2.5}}\left(\frac{v_0}{r_0}\right)\left(\frac{v_0 r_0}{\nu_f}\right)^{1/2}\left(\frac{r}{r_0}\right)^{3n-2} G'(0). \tag{2.14}$$

Eqs. (2.13) and (2.14) can be used to determined normalized skin friction C_{fr} defined below:

$$C_{fr} = \frac{\left(\tau_r^2 + \tau_\phi^2\right)^{1/2}}{\rho_f\{v_0(r/r_0)^{2n-1}\}^2}. \tag{2.15}$$

Invoking transformations (2.7), Eq. (2.15) changes to the following:

$$Re_r^{1/2} C_{fr} = \frac{\sqrt{\left(F'(0)\right)^2 + \left(G'(0)\right)^2}}{(1-\phi_1)^{2.5}(1-\phi_2)^{2.5}}, \tag{2.16}$$

where $Re_r = v_w r/\nu_f$ define s the local Reynolds number.

Cooling rate of the surface can be estimated by calculating local Nusselt number defined below:

$$Nu_r = \frac{r q_w}{k_f(T_w - T_\infty)}, \tag{2.17}$$

where $q_w = -k_{hnf}(\partial T/\partial z)_{z=0}$ represents heat flux at the surface. Using transformation (2.6), Eq. (2.17) converts to the following:

$$Re_r^{-1/2} Nu_r = -\frac{k_{hnf}}{k_f}\theta'(0). \tag{2.18}$$

Eqs. (2.16) and (2.18) clearly indicate that one has to focus on the values of $F'(0), G'(0)$ and $\theta'(0)$ to discover physical insights of the present model.

2.3 Numerical Method

For the numerical solution of the problem, Eqs. (2.8) – (2.11) are converted into a system of first-order equations by substituting $F' = Z,\ G' = P,\ \theta' = Q$. We obtain the following system:

$$H' = F, \tag{2.19}$$

$$Z' = \epsilon_1\epsilon_2\{(n+1)HZ + (1-2n)F^2 + G^2 - 1\}, \tag{2.20}$$

$$P' = \epsilon_1\epsilon_2\{(n+1)HP - 2nFG\}, \tag{2.21}$$

$$Q' = \epsilon_3\frac{k_f}{k_{hnf}}\left\{(n+1)PrHQ - 2(2n-1)Pr\,H'\theta - \frac{PrEc}{\epsilon_1\epsilon_3}(Z^2 + P^2)\right\}. \tag{2.22}$$

In order to solve Eqs. (2.19) – (2.22) with the respective conditions, we relied on the built in tool bvp4c of the commercial software MATLAB. This routine is based on the collocation method which gives continuous solution on the mesh x_i $(i = 1,2,\cdots N)$. To run the code, the value of η_∞ is set as low as 2 and then it is gradually increased until the initial values of H, F, G and θ become independent on the integration domain. The residuals in boundary condition for F, G and θ at infinity are set to stay below the specified tolerance of 10^{-6}. Table 2.3

demonstrates that our numerical results are in excellent match with those given by Rahman and Andersson [56].

Table 2.3: Comparison with results of $F'(0), G'(0)$ and $-H(\infty)$ obtained by Rahman and Andersson [56] in case of ordinary fluids when $n = 1$.

$-A$	$F'(0)$		$G'(0)$		$-H(\infty)$	
	Present	R & A [56]	Present	R & A [56]	Present	R & A [56]
0	0.94197	0.9420	0.77289	0.7729	-0.65399	-0.6747
0.5	0.83514	0.8351	1.38851	1.3885	0.13608	0.1361
1.0	0.64684	0.6468	2.1560	2.1560	0.85176	0.8518
2.0	0.36978	0.3698	4.02763	4.0276	1.97364	1.9763

2.4 Results and Discussion

We analysed hybrid nanofluid boundary layer in a generalized vortex flow subjected to viscous dissipation effect. Representative problem given by Eqs. (2.8) – (2.11) along with conditions (2.12) has been treated by a reliable computational platform bvp4c of MATLAB. To investigate flow behaviour under different controlling parameters, velocity fields represented by $F(\eta), G(\eta)$ and $H(\eta)$ and temperature profile $\theta(\eta)$ are displayed graphically (see Figs. 2.2–2.6). Results corresponding to two different scenarios namely (i) potential vortex ($n = 0$) and (ii) rigid-body rotation ($n = 1$) are computed for comparison purposes. For impermeable surface ($A = 0$), velocity curves are seen to exhibit oscillations in η and amplitude of such oscillations is inversely proportional to n, which is in accordance with the observations of Rahman and Andersson [56]. It was clearly indicated that resulting temperature profile does not fulfil the augmentation condition, that is, θ' does not vanish as $\eta \to \infty$. Figs. 2.2 and 2.3 demonstrates how suction contributes to the variation in vortex flow and resulting heat transfer with and without nanoparticles. Two important observations are drawn from these figures. Firstly, the amplitude and wavelength of oscillations are reduced as A enlarges. In fact, the oscillatory behaviour of flow fields is removed under wall suction velocity. Secondly, axial velocity becomes constant and boundary layer is incredibly suppressed for increasing A-values. As volume fractions ϕ_1 and ϕ_2 become large, a noticeable reduction in velocity profiles becomes evident. Expression of μ_{hnf} (as in Table 2.1) clearly depict an inversely linear relation between effective viscosity and volume fractions ϕ_1 and ϕ_2. Hence, an increased volume fraction leads to an enhanced viscosity coefficient which results in reduced fluid motion. Consequently, boundary layer thickness is seen to suppress as we increase either ϕ_1 or ϕ_2. As for the temperature field, the enhancement in vertical flow as a consequence of wall suction

greatly thins the thermal penetration depth which thereby elevates heat transfer rate from the solid surface. The results corresponding to $n = 0$ are displayed in Figs. 2.3 (a-d). It is noticed that variations in solutions are more prominent in the case $n = 0$ compared with that in $n = 1$.

Figs. 2.4 (a-d) demonstrate how the present flow model is influenced by the variation in power-law index n. Interestingly, the shape of velocity profiles is similar to that in pure Bodewadt flow. The striking effect of n appears to be the thickening of momentum boundary layer when n reduces, an outcome that is in accordance with [56]. Different from no suction case ($A = 0$), where we witnessed damped oscillations in the solutions, the velocity curves become monotonic function of η in case of sufficiently high suction ($A < -2.0$). At $A = -2.0$, a notable increase in radial velocity is observed as the case of potential vortex is approached. This accelerated radial motion is compensated by reduced axial motion directed towards the surface. Circular motion also intensifies whenever n is reduced. The presence of nanoparticles is seen to have an effect of resisting fluid motion, since Figs. 2.4 (a-c) clearly depict a decreasing trend in velocity components for increasing volume fraction. As anticipated, a marked growth is thermal penetration depth is found for increasing volume fraction (see Fig. 2.4(d)). The reduction in axial flow upon reducing n weakens heat convection process measured by the term $w\partial T/\partial z$ in energy equation and, consequently, an elevation in thermal boundary layer thickness is witnessed through Fig. 2.4 (d).

Figs. 2.5 (a) and 2.5 (b) demonstrate the change in temperature profile when $n = 0$ and $n = 1$ respectively, by keeping suction parameter fixed at $A = -2.0$. At higher Pr-values, temperature profiles require smaller distances to approach ambient condition. This is because, a larger Prandtl number fluid has relatively lower thermal diffusivity and hence thermal boundary layer thickness cannot be as high as for smaller Prandtl number fluid. A comparison of Figs. 2.5 (a) and 2.5 (b) clearly shows that, in the case of potential vortex ($n = 0$), thermal boundary layer is much broader than that in the case of Bödewadt flow.

Figs.2.6 (a) and 2.6 (b) include temperature profiles for varying choices of Eckert number Ec. Viscous dissipation refers to the heat generation in boundary layer as a result of shearing forces. An important observation is that deviation in temperature profile with addition of nanoparticles is higher at $n = 0$ than at $n = 1$. Also, viscous dissipation seems to have a prominent role at $n = 0$, compared with that at $n = 1$. Thermal boundary layer is markedly elevated due to the inclusion of viscous dissipation term.

Representative results for radial and azimuthal skin frictions are included in Table 2.4 for varying choices of embedded parameters. When n enlarges, both radial and azimuthal stresses at the disk are significantly enhanced, thereby elevating the normalized wall skin friction. Drag experienced at the surface is much enhanced due to an increase in wall suction velocity. Role of nanoparticles on the normalized wall skin friction can be understood from Eq. (2.16), where ϕ_1 and ϕ_2 appear to be proportional to C_f. As a result, larger drag coefficient occurs whenever higher volume fraction is considered.

Table 2.5 lists local Nusselt number data at different choices of controlling parameters. Heat transfer rate is predicted to lower as the case of potential vortex is approached. However, the action of wall suction incredibly improves heat transfer rate as witnessed from first four entries of Table 2.5.

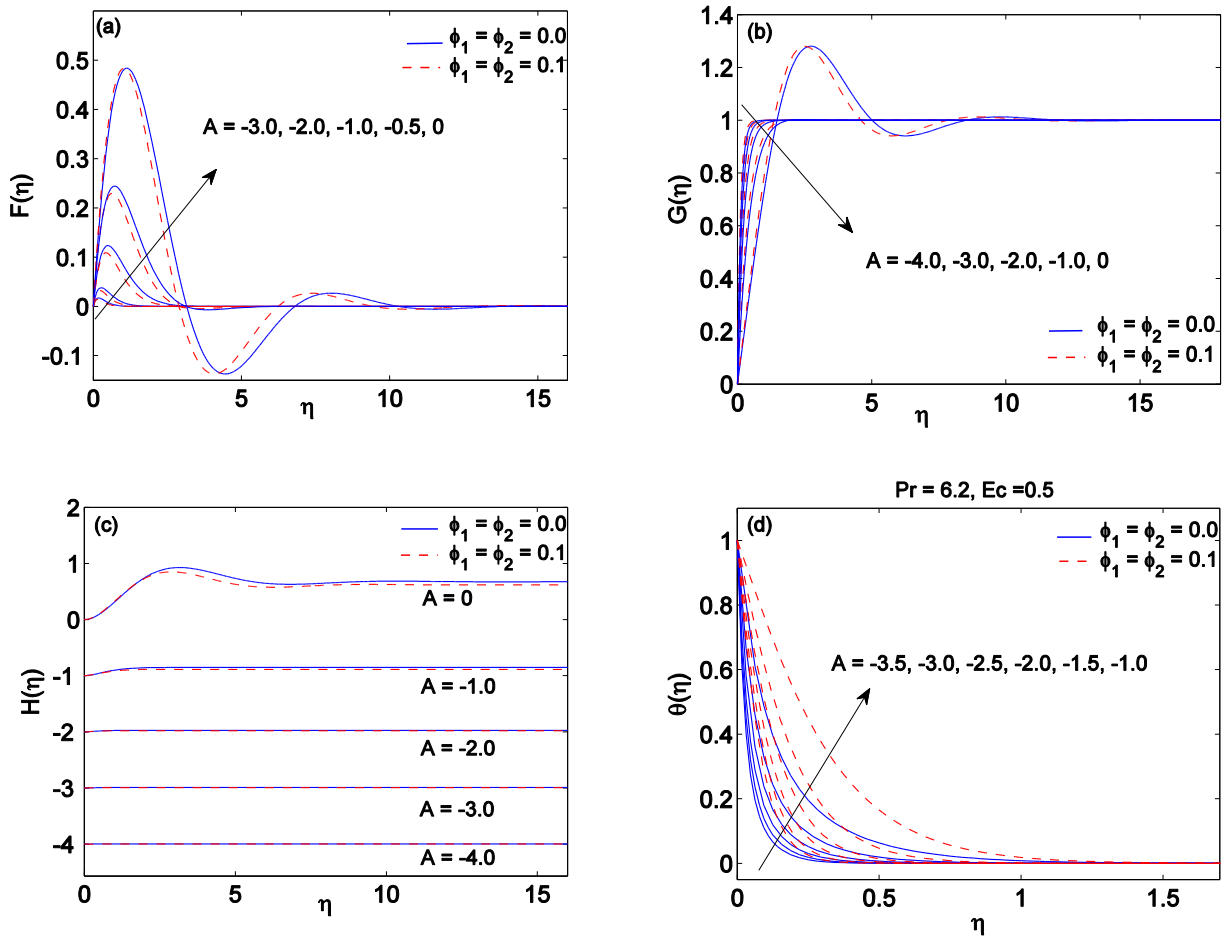

Fig. 2.2 (a-d): Change in velocity components (F, G, H) and temperature (θ) with η for varying choices of wall suction parameter A when $n = 1$.

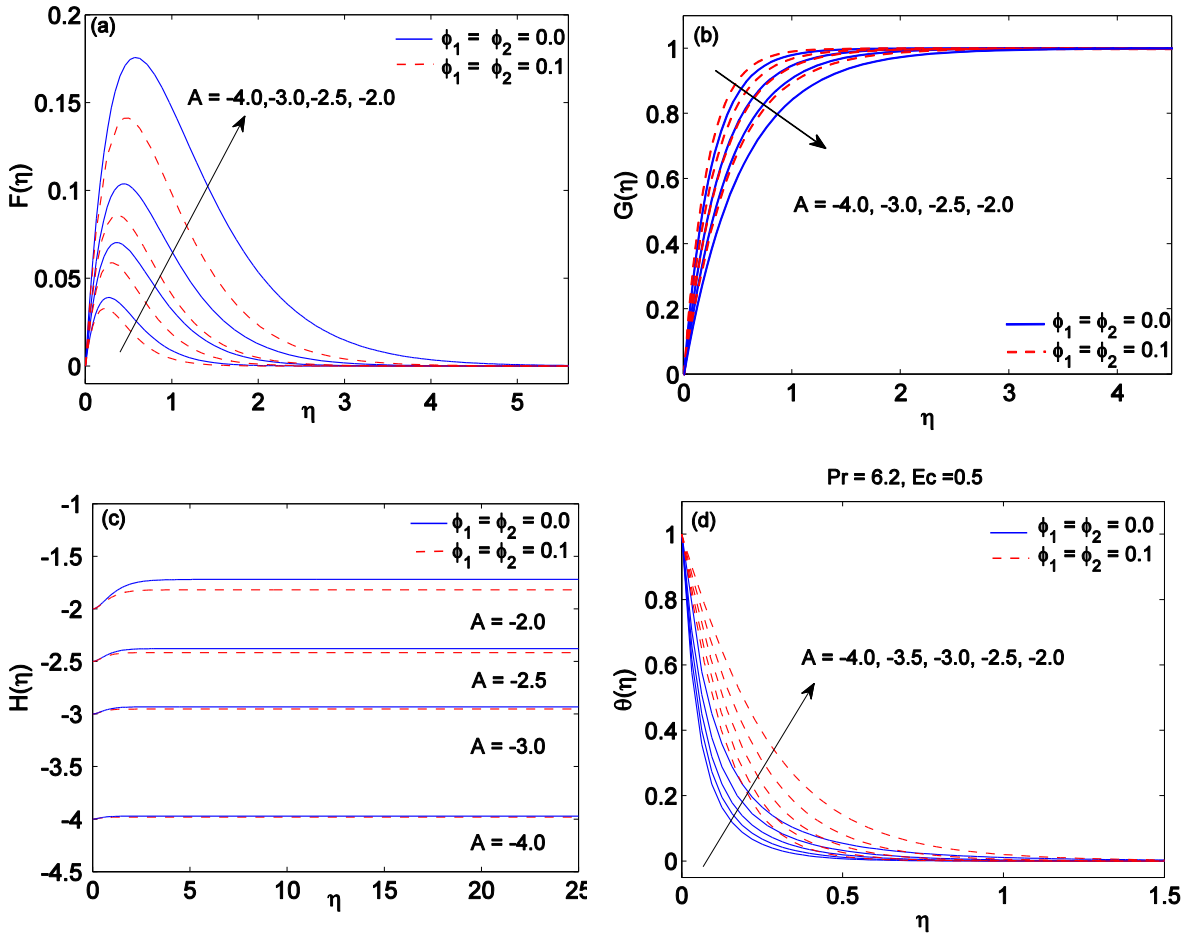

Fig. 2.3 (a-d): Change in velocity components (F, G, H) and temperature (θ) with η for varying choices of wall suction parameter A when $n = 0$.

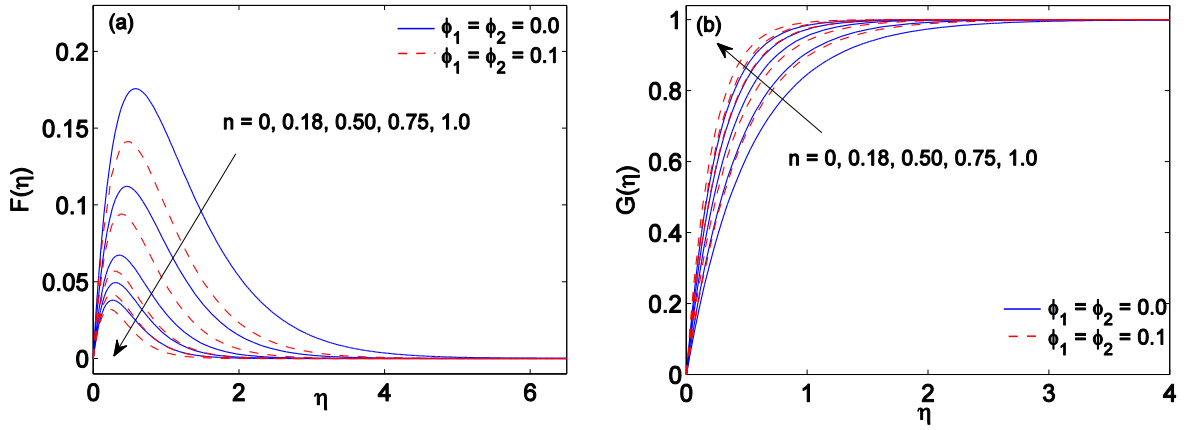

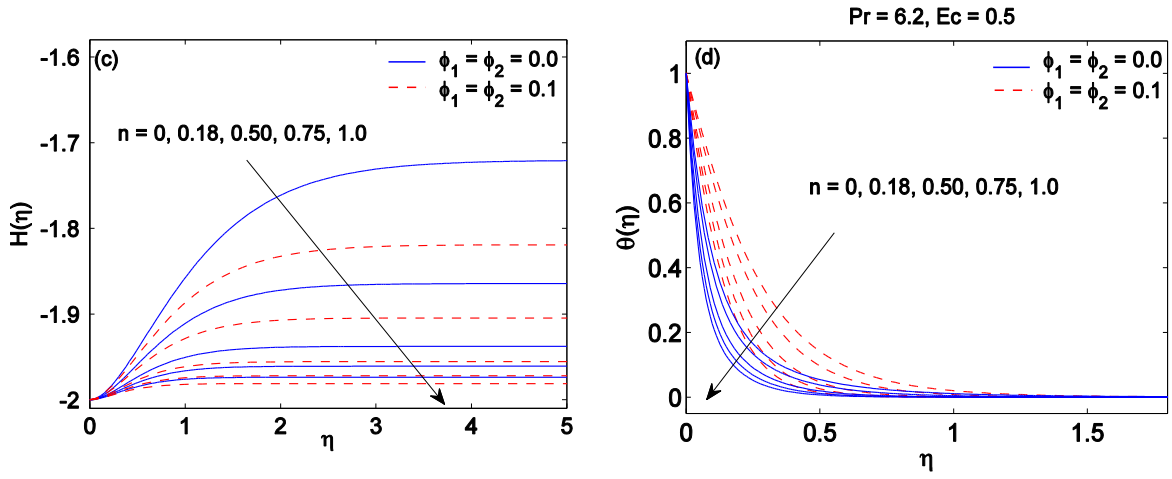

Fig. 2.4 (a-d): Change in velocity components (F, G, H) and temperature (θ) with η for varying choices of power law index n when $A = -2.0$.

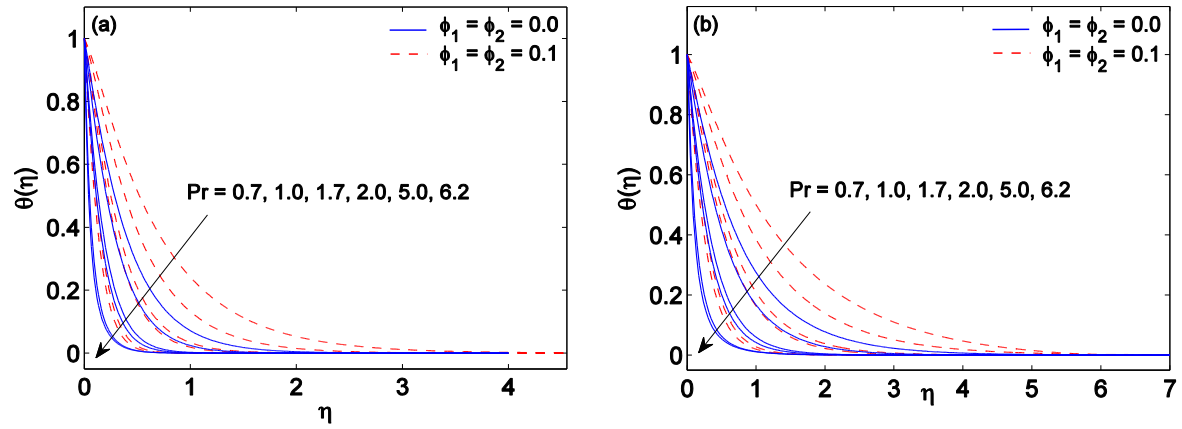

Fig. 2.5: Temperature curves at different Prandlt number Pr-values when (a) $n = 1$ and (b) $n = 0$ with suction $A = -2.0$ *and* $Ec = 0.5$.

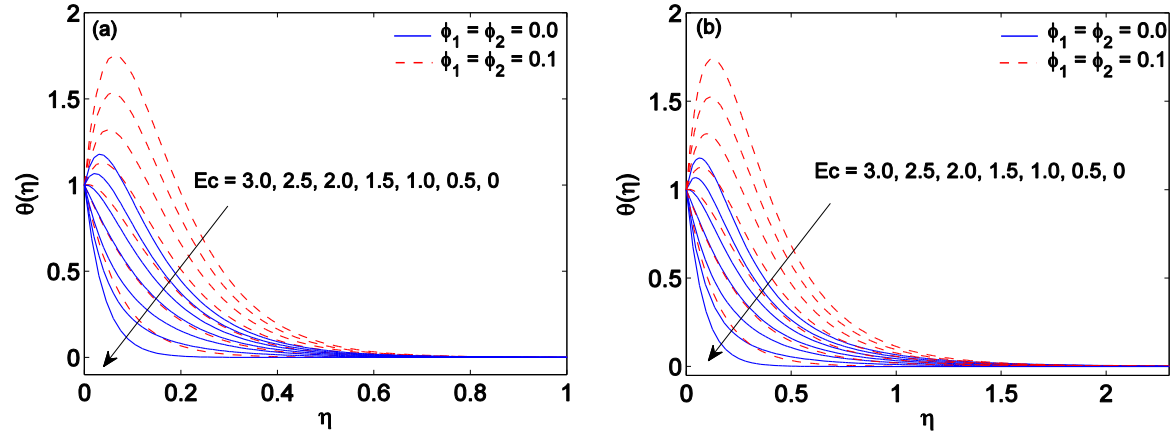

Fig. 2.6: Temperature curves at different Eckert number Ec-values when (a) $n = 1$ and (b) $n = 0$ with suction $A = -2.0$, $Pr = 6.2$.

Table 2.4: Results of normalized wall skin friction for varying choices of A and n when $\phi_1 = \phi_2 = 0.1$.

$-A$	n	$\frac{F'(0)}{(1-\phi_1)^{2.5}(1-\phi_2)^{2.5}}$	$\frac{G'(0)}{(1-\phi_1)^{2.5}(1-\phi_2)^{2.5}}$	$\frac{\sqrt{F'(0)^2+G'(0)^2}}{(1-\phi_1)^{2.5}(1-\phi_2)^{2.5}}$
0.0	1.0	1.173984	1.427539	2.250572
1.0		1.131392	4.270588	4.417915
2.0		0.628726	8.097596	8.121967
3.0		0.422517	12.09879	12.106537
4.0		0.317328	16.12079	16.123926
2.0	0.0	1.332009	3.944808	4.163623
	0.18	1,077440	4.754577	4.873482
	0.50	0.836579	6.079815	6.137102
	0.75	0.717299	7.091618	7.127802

Table 2.5: Results of Nusselt number for different choices of A, n and ϕ with $Pr = 6.2$ and $Ec = 0.5$.

$-A$	n	$\phi_1 = \phi_2 = \phi$	$-\frac{\kappa_{hnf}}{\kappa_f}\theta'(0)$
1	0.5	0.1	1.575979
1.5			3.521862
2			5.014561
2.5			6.382916
2.0	0	0.1	3.408955
	0.3		4.329415
	0.6		5.362934
	1.0		6.766857
2.0	0.5	0.0	14.755562
		0.03	10.839275
		0.06	7.8779813
		0.1	5.014584

2.5 Concluding Remarks

The numerical solution developed for vortex flow of hybrid nanofluid over a permeable surface has enabled us to figure out the consequences of nanoparticles and viscous dissipation on the solution profiles. Notable outcomes of this research are outlined below:

- The accuracy of numerical solutions deteriorates as the case of potential vortex is approached. Indeed, for potential vortex case, one needs to consider sufficiently high suction velocity to make bvp4c code workable. For Bödewadt flow ($n = 1$), numerical solution for velocity profiles is possible even in no suction case.

- In no suction case, axial motion is directed upwards while its direction is reversed when sufficiently large suction velocity is considered. In a previous paper, it has already been demonstrated that only downward axial flow can give meaningful temperature profile.
- Radially inward motion as well as tangential flow are predicted to accelerate whenever n is decreased. This reduction is compensated by an enhanced axial flow towards the surface.
- The addition of nanoparticles restricts the fluid motion and, consequently, boundary layer becomes incredibly thinner as nanoparticle volume fraction enlarges.
- It is natural to witness that thermal penetration depth expands whenever volume fraction ϕ is enhanced. As a result, wall temperature gradient is lowered upon increasing ϕ.
- For increasing Eckert number Ec-values, it requires larger value of η for temperature profile to reach its asymptotic value. This behaviour accompanies with lower slope of temperature profile at the surface.

Chapter 3

A study of Heat and Mass Transfer on Generalized Vortex Flow Using Buongiorno Model

3.1 Introduction

This chapter investigates generalized vortex flow over a plane permeable surface using two-phase Buongiorno model. Velocity of the tangential flow is assumed to be proportional to r^m, where r is radial coordinate and m denotes the power-law index. The diffusion coefficients are not assumed constant here. A set of transformations is adopted, which transforms the governing problem into a coupled differential system, whose numerical solution is developed by MATLAB's package bvp4c. Simulations are made by assuming a power-law surface temperature distribution. Present model reduces to two special situations namely rigid body rotation ($m = 1$) and potential vortex ($m = -1$). The contribution of Brownian diffusion and Soret effect on the vortex induced motion is studied. Furthermore, interesting fluid dynamics entities such as resisting wall shear and heat transfer rate are also deliberated.

3.2. Mathematical Modelling

We are concerned with flow situation involving an incompressible nanofluid above a stationary disk infinite in extent occupying the plane $z = 0$. Let u, v and w represent the velocity vector projections along the radial $r-$, azimuthal $\varphi-$ and axial $z-$ directions respectively. Tangential flow far above the disk is in a state of rotation with velocity proportional to r^m, where $m = 2n - 1$ denotes prescribed parameter. Resulting heat transfer due to variable surface temperature of the form $T_w = T_\infty + (r/r_0)^{2m}$ is considered, where r_0 is a constant. Rotationally symmetric assumption of the flow field renders the variation in velocity with φ is negligible. Here, Buongiorno model is utilized with temperature dependence of diffusion coefficients being retained. In existence of frictional heating, the aforementioned problem is described by the following set of PDEs:

$$\frac{\partial}{\partial r}(ru) + \frac{\partial}{\partial z}(rw) = 0, \tag{3.1}$$

$$u\frac{\partial u}{\partial r} - \frac{v^2}{r} + w\frac{\partial u}{\partial z} = -\frac{1}{\rho_{nf}}\frac{\partial p}{\partial r} + \nu_{nf}\left(\frac{\partial^2 u}{\partial z^2}\right), \tag{3.2}$$

$$u\frac{\partial v}{\partial r} + \frac{uv}{r} + w\frac{\partial v}{\partial z} = \nu_{nf}\left(\frac{\partial^2 v}{\partial z^2}\right), \tag{3.3}$$

$$(\rho C_p)_{nf}\left(u\frac{\partial T}{\partial r}+w\frac{\partial T}{\partial z}\right)=k_{nf}\frac{\partial^2 T}{\partial z^2}+\mu_{nf}\left\{\left(\frac{\partial u}{\partial z}\right)^2+\left(\frac{\partial v}{\partial z}\right)^2\right\}+\rho_p C_p\left\{C_B\,T\frac{\partial \phi}{\partial z}\frac{\partial T}{\partial z}+C_T\frac{\phi}{T}\left(\frac{\partial T}{\partial z}\right)^2\right\}, \tag{3.4}$$

$$u\frac{\partial \phi}{\partial r}+w\frac{\partial \phi}{\partial z}=\frac{\partial}{\partial z}\left(C_B T\frac{\partial \phi}{\partial z}+C_T\frac{\phi}{T}\frac{\partial T}{\partial z}\right). \tag{3.5}$$

and subjected to the boundary conditions:

$$\begin{gathered} u=0,\ v=0,\ w=w_0(r),\ \ T=T_w(r),\ C_B T\nabla\phi+C_T\phi\frac{\nabla T}{T}=0 \text{ at } z=0,\\ u\to 0,\ v\to v_\infty=v_0(\tfrac{r}{r_0})^{2n-1},\ T\to T_\infty,\ \phi\to\phi_\infty \text{ as } z\to\infty. \end{gathered} \tag{3.6}$$

where, $w_0(r)=Av_0(\nu_f/v_0r_0)^{1/2}(r/r_0)^{n-1}(n+1)$ and $\rho_{nf},\nu_{nf},(\rho C_p)_{nf},k_{nf}$, are effective density, kinematic viscocity, volumetric heat capacity and thermal conductivity of nanofluids respectively. Here we do not consider variation in volume fraction and hence set these properties to new parameters at far-field as $\rho_\infty,\nu_\infty,(\rho C_p)_\infty,k_\infty$.

Furthermore, as per Buongiorno [16] considered $C_B=(D_B/T)$ and $C_T=(D_T/\phi)$ as diffusion parameters, Such dependency was ignored in the past papers without proper physical explanation.

Invoking the following similarity transformations [56]:

$$\begin{gathered} u(r,z)=-v_0\left(\frac{r}{r_0}\right)^{2n-1}F(\eta),\ \ v(r,z)=v_0\left(\frac{r}{r_0}\right)^{2n-1}G(\eta),\\ w(r,z)=Av_0\left(\frac{\nu_\infty}{v_0r_0}\right)^{1/2}\left(\frac{r}{r_0}\right)^{n-1}\left[(n+1)H(\eta)+(n-1)\eta F(\eta)\right],\\ p(r)=\frac{\rho_\infty {v_0}^2}{4n-2}\left(\frac{r}{r_0}\right)^{4n-2},\ \ T(r,z)=T_\infty+\Delta T\theta(\eta),\ \ \phi(r,z)=\phi_\infty+\phi_\infty\chi(\eta).\\ \text{with } \eta=\left(\frac{z}{r_0}\right)\left(\frac{r}{r_0}\right)^{n-1}\left(\frac{v_0r_0}{\nu_\infty}\right)^{1/2}, \end{gathered} \tag{3.7}$$

The governing equations (3.1) – (3.5) will be of the form:

$$H'-F=0, \tag{3.8}$$

$$F''-(n+1)HF'-(1-2n)F^2-G^2+1=0, \tag{3.9}$$

$$G''-(n+1)HG'+2nFG=0, \tag{3.10}$$

$$\frac{1}{Pr}\theta''-(n+1)H\theta'+2(2n-1)\,H'\theta+\ Ec\left(F'^2+G'^2\right)+Nt(1+\chi)(\theta')^2+Nb\chi'\theta'=0, \tag{3.11}$$

$$\chi''+\frac{\Delta T}{T_\infty}\theta'\chi'+\frac{Nt}{Nb}\left(\theta'\chi'+(1+\chi)\theta''-(1+\chi)(\theta')^2\frac{\Delta T}{T_\infty}\right)-(n+1)ScH\chi'=0. \tag{3.12}$$

where $\Delta T=(T_w-T_\infty)$, Pr defines base fluid Prandlt number, Ec represents Eckert number, Nt and Nb denotes the Brownian and thermophoresis parameters and Sc defines Schmidt number. Buongiorno [16] also assumed that $\Delta T\ll T_\infty$ which enables us to write $\Delta T\theta(\eta)+T_\infty$ as T_∞ while deriving Eqs. (3.9) – (3.12). All the dimensionless parameters are defined as:

$$Pr = \frac{(\rho C_p)_\infty \nu_\infty}{k_\infty}, \quad Ec = \frac{{v_\infty}^2}{(C_p)_\infty \Delta T} \text{ with } v_\infty = v_0 \left(\frac{r}{r_0}\right)^{(2n-1)},$$
$$Nt = \frac{C_T \phi_\infty \Delta T \rho_p C_p}{T_\infty \nu_\infty (\rho C_p)_\infty}, \quad Nb = \frac{C_B T_\infty \phi_\infty \rho_p C_p}{\nu_\infty (\rho C_p)_\infty}, \quad Sc = \frac{\nu_\infty}{C_B T_\infty}. \tag{3.13}$$

Now the boundary conditions (3.6) will transform to:

$$F = 0, \ G = 0, \ H = A, \ \theta = 1, \ \chi' + \frac{Nt}{Nb}(1+\chi)\theta' = 0 \quad \text{at} \quad \eta = 0,$$
$$F \to 0, \ G \to 1, \ \theta \to 0, \ \chi \to 0 \quad \text{as} \quad \eta \to \infty. \tag{3.14}$$

The radial and tangential shear stresses at the surface are calculated as follows:

$$\tau_r = \mu_{nf} \left(\frac{\partial u}{\partial z}\right)_{z=0} = -\mu_\infty \left(\frac{v_0}{r_0}\right) \left(\frac{v_0 r_0}{\nu_\infty}\right)^{1/2} \left(\frac{r}{r_0}\right)^{3n-2} F'(0),$$
$$\tau_\phi = \mu_{nf} \left(\frac{\partial v}{\partial z}\right)_{z=0} = \mu_\infty \left(\frac{v_0}{r_0}\right) \left(\frac{v_0 r_0}{\nu_\infty}\right)^{1/2} \left(\frac{r}{r_0}\right)^{3n-2} G'(0). \tag{3.15}$$

Eqs. (3.15) can be used to determine normalized skin friction C_{fr} defined below:

$$C_{fr} = \frac{(\tau_r^2 + \tau_\phi^2)^{1/2}}{\rho_f \{v_0 (r/r_0)^{2n-1}\}^2}, \tag{3.16}$$

Using transformations (3.7), Eq. (3.16) changes to the following:

$$Re_r^{1/2} C_{fr} = \sqrt{(F'(0))^2 + (G'(0))^2}. \tag{3.17}$$

where $Re_r = v_w r / \nu_\infty$ defines the local Reynolds number.

Cooling rate of the surface can be estimated by calculating local Nusselt number defined below:

$$Nu_r = \frac{r q_w}{k_\infty (T_w - T_\infty)}, \tag{3.18}$$

where $q_w = -k_\infty (\partial T / \partial z)_{z=0}$ represents heat flux at the surface. By transformation (3.7), Eq. (3.18) converts to the following:

$$Re_r^{-1/2} Nu_r = -\theta'(0). \tag{3.19}$$

3.3 Results and Discussion

Thermal transport in generalized vortex flow involving nanofluid is investigated by using Buongiorno's model. The approach outlined above is utilized to generate numerical data for unknown functions (3.9) – (3.12), in the range $0 \leq n \leq 1$.

In Figs. 3.1 (a-c), we present variations in velocities (u, v, w) and temperature (T) as the power-law index n changes. Near the surface, frictional effects tend to slow down the induced circumferential motion. Resultantly, fluid particles near the disk are being pushed towards the

axis of rotation ($r = 0$) under radial pressure gradient, which was employed far from the disk to accomplish the desired vortex motion. The inward radial motion around the surface creates an intriguing axial flow (directed upwards), to satisfy the mass conservation constraint. However, the direction of axial motion reverses when sufficiently large value of A is invoked. Without permeability assumption, velocity components have oscillatory profiles as demonstrated by Rahman and Andersson [56]. It is worth stating that accuracy of bvp4c code deteriorates as the case of potential vortex is approached. In fact, for $n = 0$, solutions could only be possible where boundary is subjected to sufficient suction velocity. General trend of velocity distributions is preserved for all values of n. Boundary layer progressively develops as one approaches the case of potential vortex ($n = 0$). Precisely, radial flow accelerates while tangential and axial motions slow down whenever n is reduced.

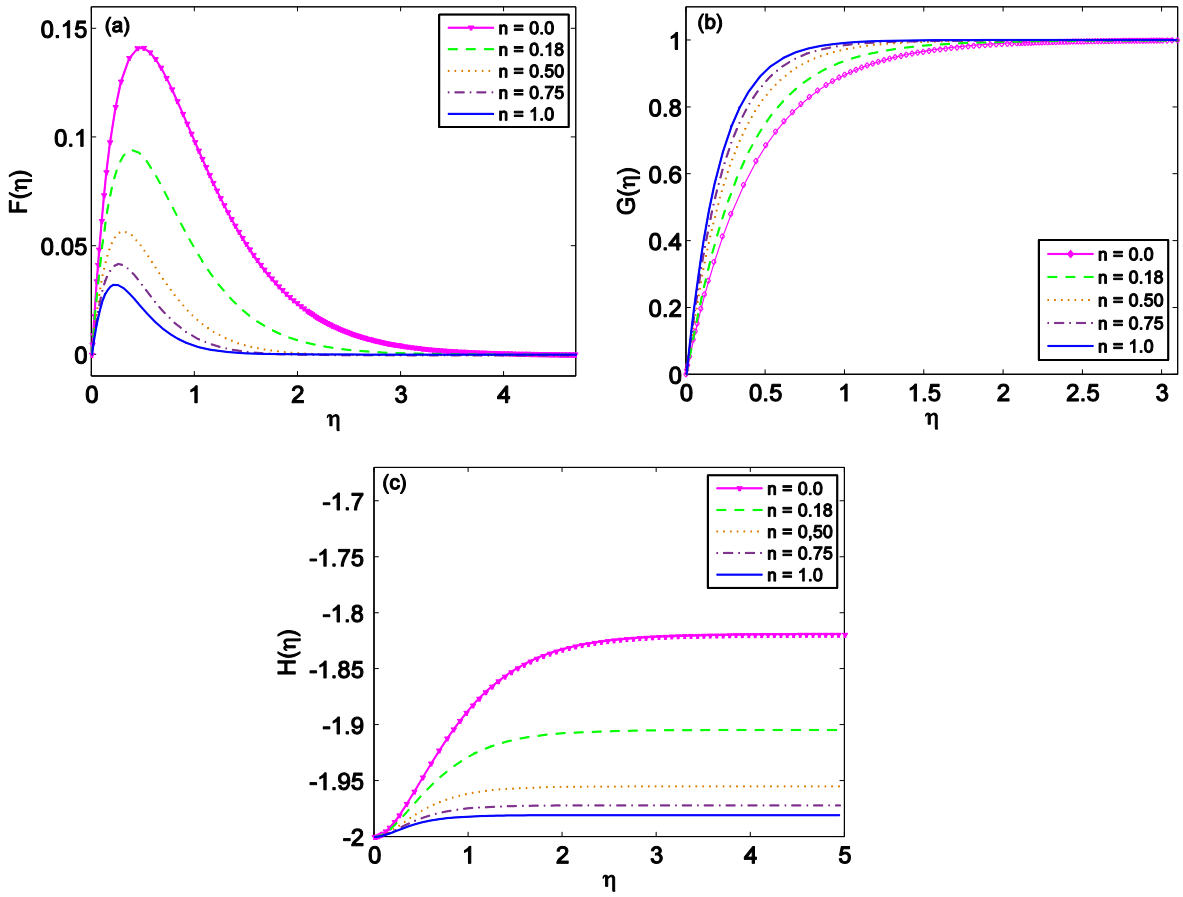

Fig. 3.1 (a-c): Change in velocity components (F, G, H) with η for varying choices of power law index n when $A = -2.0$.

To understand the heat transfer process in nanoparticle working fluid undergoing vortex induced motion, we prepare graphs of θ versus η by changing the controlling parameters (see Figs. 3.2 (a-e). Fig. 3.2(a) suggests that action of wall suction incredibly suppresses the

θ −profile thereby elevating heat transfer rate at the surface. This result arises because a higher volume of fluid (with comparatively lower temperature) is being pushed towards the disk under wall suction effect. Also, a notable growth in thermal penetration depth is witnessed for decreasing n-values. Physically, the accelerated axial flow increases convection effect measured by the quantity $w\partial T/\partial z$, which consequently leads to a thinner temperature profile (see Fig. 3.2 (b)). Fig. 3.2 (c) exhibits the role of varying Prandtl number on resulting heat transfer. By definition, Prandtl number shows the ratio of convection to pure conduction. Therefore, fluids with larger Prandtl number have higher heat transfer rate but lower thermal conduction ability. As a result, we notice a considerable decline in temperature profiles for increasing Pr-values. The behaviour of thermophoretic diffusion (or Soret effect) on temperature curve is exhibited in Fig. 3.2 (d). Fluid particles surrounding the disk are heated due to which they acquire relatively higher kinetic energy with their higher temperature. Such fluid particles collide with nanoparticles and drive the later away from the disk. For increasing Nt-values, thermophoretic diffusion intensifies, due to which nanoparticles acquire a higher extent of the fluid. Resultantly, thermal boundary layer expands and temperature curve becomes broader as in Fig. 3.2 (d). The effect that viscous dissipation terms can have on the considered vortex motion can be predicted via Fig. 3.2 (e). It is clear that ignoring viscous heating in such scenarios could have a considerable influence on the related outcomes. An important observation is that the contribution of viscous dissipation diminishes in the two limiting cases $Pr \to 0$ and $Pr \to \infty$. Eckert number Ec measures the importance of fluid's kinetic energy relative to the enthalpy difference. Consequently, increasing Ec-values leads to higher average kinetic energy and hence larger temperature function. For sufficiently high value of Ec, the so-called Sparrow-Gregg Hill (SGH) is visible indicating a physically unacceptable situation.

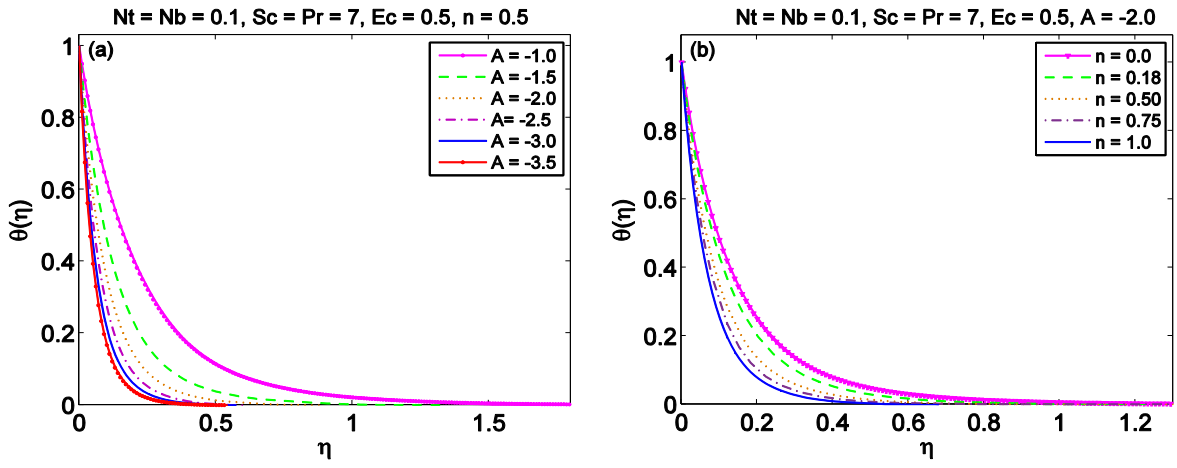

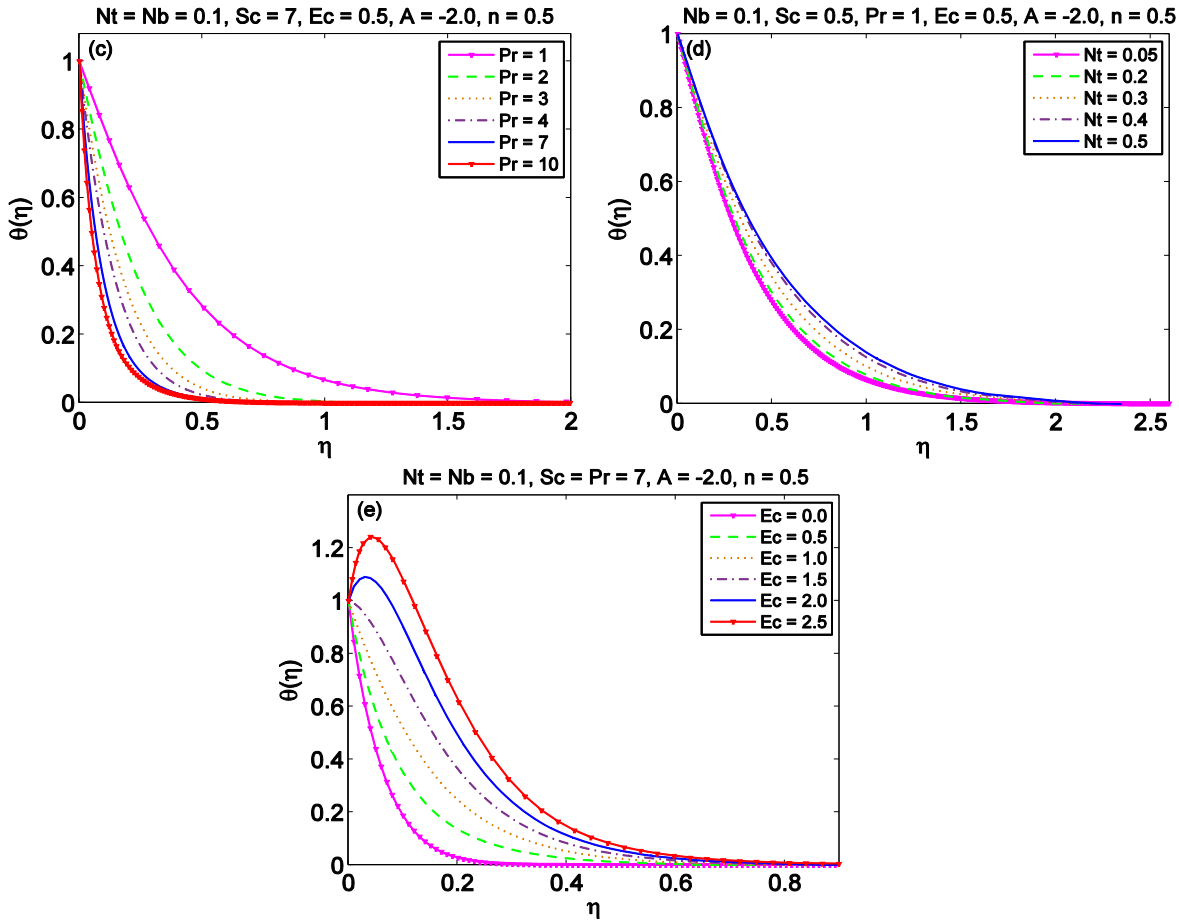

Fig. 3.2 (a-e): Variation in temperature profile $\theta(\eta)$ for varying choices of parameters.

Curves of concentration distribution under various controlling parameters have been shown in Figs. 3.3 (a-e). Concentration function ϕ is negative at the disk which depicts that concentration within the wall becomes higher than that of the wall. General trend of concentration curve is that it first rises to a maximum as η increases and then asymptotes to zero as $\eta \to \infty$. Concentration distribution becomes thinner as we increase the wall suction parameter A. Role of parameter n on the concentration profile is shown in Fig. 3.3 (b). Similar to the temperature profile, concentration profile becomes broader in transition from the Bödewadt flow to the potential vortex situation. Fig. 3.3 (c) illustrates that it requires lesser vertical distance for concentration ϕ to approach zero when larger Schmidt number Sc is chosen. Physically, Schmidt number is a measure of ratio of momentum diffusion to mass diffusion. For increasing Sc-values, mass diffusion rate reduces which thereby suppresses concentration boundary layer. Furthermore, the effect of thermophoresis is such that nanoparticles with relatively higher thermal conductivity migrate away from the disk thereby providing enhancement in concentration boundary layer (see Fig. 3.3 (d)). Lastly, we have investigated the variation of Nb in Fig.3.3 (e) that thickens the volume fraction boundary layer that is of the same effects as of the Nt.

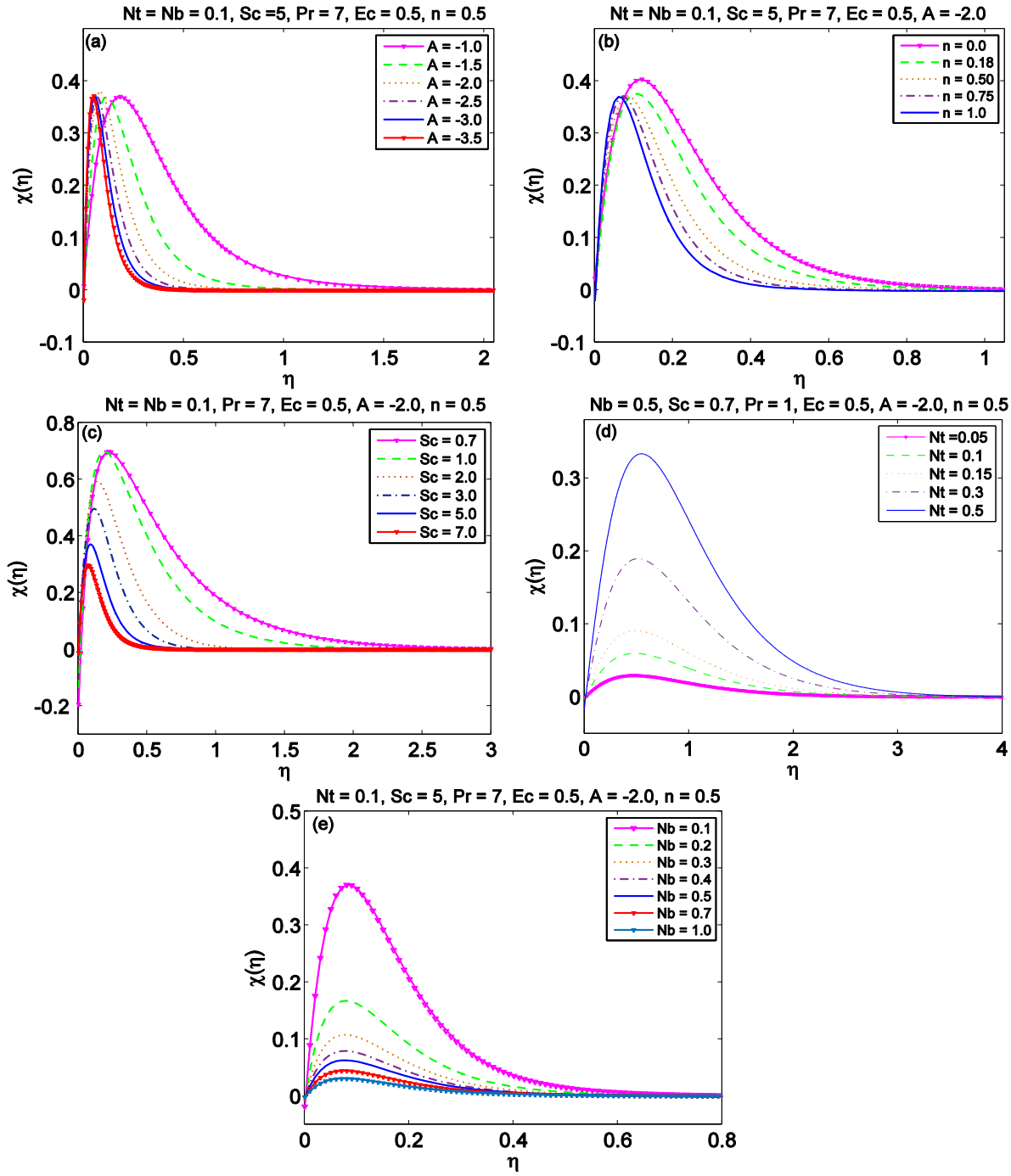

Fig. 3.3 (a-e): Variation of concentration profile $\chi(\eta)$ for varying choices of parameters.

Results of Nusselt number and wall concentration gradient are represented in Tables 3.1 and 3.2 for varying choices of parameters. It is detected that heat transfer rate incredibly improves whenever wall suction velocity enlarges. Also, thermophoresis or Soret effect has a substantial contribution towards improvement in heat transfer rate. Increasing Eckert number values Ec leads to more heat loss which in turn lowers heat transfer rate at the disk. Also, a marked reduction in heat transfer rate is observed for decreasing n-values. Wall concentration gradient

measured by the term $\phi'(0)$ also declines whenever n is lowered. However, it has risen sharply under increasing Soret effect.

Table 3.1: Results of Nusselt number for varying choices of Pr, Sc, Nt, Ec, n and A with $Nb = 0.1$.

Pr	Sc	Nt	Ec	n	$-A$	$-\theta'(0)$
1	7	0.1	0.5	0.5	2.0	2.0819
2						4.0247
4						7.6423
7						12.7264
9						16.0017
1	0.7	0.1				2.1298
		0.2				2.0189
		0.3				1.8518
		0.4				1.6202
		0.5				1.3432
7	7	0.1	0			17.0923
			0.5			12.7264
			1			8.0416
			1.5			3.0108
			0.5	0		8.5160
				0.18		9.9872
				0.75		14.8903
				1		17.0571
				0.5	1.0	5.4519
					2.0	12.7264
					3.0	19.2870
					4.0	25.7616

Table 3.2: Results of wall concentration gradient for varying choices of Sc, Nt, Nb, Pr, n and A with $Ec = 0.5$.

Sc	Nt	Nb	Pr	n	$-A$	$\chi'(0)$
0.7	0.1	0.1	7	0.5	2.0	12.0222
1.0						12.6870
7.0						12.5554
9.0						12.3944
0.7	0.05	0.5	1			0.2168
	0.1					0.4266
	0.15					0.6292
	0.3					1.1908
	0.5					1.8217
5	0.1	0.2	7			6.5700
		0.5				2.6674
		0.7				1.9104
		1				1.3400

		0.1	7	0		8.5948
				0.18		10.0492
				0.75		14.9424
				1		17.1099
				0.5	1.0	5.6202
					2.0	12.7797
					3.0	19.3379
					4.0	25.8227

3.4 Concluding Remarks

Here we worked out the computational results for induced vortex motion of nanoparticle working fluid utilizing Buongiorno model. Results indicate that wall suction has pivotal role in physically acceptable solution of the transport equations. Significant outcomes of present research are outlined as follows:

- Our calculations detected that the developed problem is self-similar only if temperature difference $(T_w - T_\infty)$ is proportional to $(r/r_0)^{2n}$, otherwise the problem is only locally similar.
- Without wall suction, the accuracy of numerical solutions deteriorates as we decrease the power-law index n. Indeed, numerical solution via bvp4c is not possible in case of potential vortex when $A = 0$.
- In line with available literature, Brownian diffusion effect on temperature profile is absent whenever zero particle flux condition is treated.
- Heat transfer rate becomes considerably less in transition from Bödewadt flow to the potential vortex case.
- At some point in the boundary layer, nanoparticle concentration becomes higher than that at the wall and it is illustrated by negative value of ϕ at the disk.

Bibliography

1. H. Masuda, A. Ebata, K. Teramae, N. Hishinuma, Alteration of thermal conductivity and viscosity of liquid by dispersing ultra-fine particles (dispersion of C-Al2O3, SiO2 and TiO2 ultra-fine particles), NetsuBussei (in Japanese) 4 (1993) 227–233.
2. J. A. Eastman, S. U. S. Choi, S. Li, W. Yu and L. Thompson, Anomalously increased effective thermal conductivity of ethylene glycol based nanofluids containing copper nanoparticles, Appl. Phys. Lett. 78 (2001) 718-720.
3. C. J. Ho, J. B. Huang, P. S. Tsai and Y. M. Yang, Preparation and properties of hybrid water-based suspension of Al_2O_3 nanoparticles and MEPCM particles as functional forced convection fluid, Int. Commun. Heat & Mass Transfer 37 (2010) 490-494.
4. S. Suresh, K. P. Venkitaraj, P. Selvakumar and M. Chandrasekar, Synthesis of $Al_2O_3 - Cu$/water hybrid nanofluid using two step method and its thermophysical properties**,** Colloids Surfaces A: Physicochem. & Engg. Aspects 388 (2011) 41-48.
5. S. Suresh, K. P. Venkitaraj, P. Selvakumar and M. Chandrasekar, Effect of $Al_2O_3 - Cu$/water hybrid nanofluid in heat transfer, Exp. Therm. Fluid Sci. 38 (2012) 54–60.
6. J. Sarkar, P. Ghosh and A. Adil, A review on hybrid nanofluids, recent research, development and applications, Renew. & Sust. Energy. Rev. 43 (2015) 164-177.
7. G. Huminic and A. Huminic, Hybrid nanofluids for heat transfer applications – A state-of the art review, Int. J. Heat & Mass Transfer 125 (2018) 82-103.
8. S. S. U. Devi and S. P. A. Devi, Heat transfer enhancement of $Cu - Al_2O_3$/water hybrid nanofluid flow over a stretching sheet, J. Nigerian Math. Soc. 36 (2017) 419–433.
9. I. Waini, A. Ishak and I. Pop, Flow and heat transfer along a permeable stretching/shrinking curved surface in a hybrid nanofluid, Phys. Scr. 94 (2019) Article ID:105219.
10. M. Sheikholeslami, Numerical approach for MHD Al_2O_3-water nanofluid transportation inside a permeable medium using innovative computer method, Comput. Math. Appl. Mech. & Engg. 344 (2019) 306–318.
11. M. Sheikholeslami, M. Jafaryar, Jagar A. Ali, S. M. Hamad, A. R. Divsalar, A. Shafee, T. Nguyen-Thoi and Z. Li, Simulation of turbulent flow of nanofluid due to existence of new effective turbulator involving entropy generation, J. Mol. Liquids 291 (2019) Article ID:111283.

12. M. Sheikholeslami, R. Haq, A. Shafee, Z. Li, Y. G. Elaraki and I. Tlili, Heat transfer simulation of heat storage unit with nanoparticles and fins through a heat exchanger, Int. J. Heat & Mass Transfer 135 (2019) 470-478.
13. Waini, A. Ishak and I. Pop, Hybrid nano fluid flow and heat transfer over a permeable biaxial stretching/shrinking sheet, Int. J. Numer. Methods Heat & Fluid Flow (2019) https://doi.org/10.1108/HFF-07-2019-0557.
14. I. Waini, A. Ishak and I. Pop, Flow and heat transfer of a hybrid nanofluid past a permeable moving surface, Chinese J. Phys. (2020), doi: 10.1016/j.cjph.2020.04.024.
15. A. Jamaludin, K. Naganthran, R. Nazar and I. Pop, MHD mixed convection stagnation-point flow of Cu-Al_2O_3/water hybrid nanofluid over a permeable stretching/shrinking surface with heat source/sink, European J. Mech. / B Fluids 84 (2020) 71–80.
16. J. Buongiorno, Convective transport in nanofluids, ASME J. Heat Transfer, 128(3) (2006) 240–250.
17. U. T. Bödewadt and D. Dreh stromunguber festem.Grand, Z. Angew. Math. Mech. 20 (1940) 241-253.
18. G. K Batchelor, Note on the class of the solutions of the Navier-Stokes equations representing steady non- rotationally symmetric flow, Quart. J. Appl. Math.4 (1951) 29-41.
19. D. M. Hannah, Forced flow against a rotating disk, ARC-RM 2772 (1952).
20. G. Nath, B.J. Venkatachala, The effect of suction on boundary layer for rotating flows with or without magnetic field, Proc. Indian Acad. Sci.-Sect. A 85 (1977) 332–337.
21. B. Sahoo, Effects of slip on steady Bödewadt flow and heat transfer of an electrically conducting non-Newtonian fluid, Commun. Nonlinear Sci. & Numer. Simulat. 16 (2011) 4284-4295.
22. B. Sahoo, Steady Bödewadt flow of a Non-Newtonian Reiner-Rivlin Fluid, Diff. Eqs. & Dynam. Syst. 20 (2012) 367-376.
23. M. Turkyilmazoglu, Bödewadt flow and heat transfer over a stretching stationary disk, Int. J. Mech. Sci. 90 (2015) 246-250.
24. P. T. Griffiths, S. J. Garrett, S. O. Stephen and Z. Hussain, Quantifying non-Newtonian effects in rotating boundary-layer flows, European J. Mech. –B/Fluids. 61 (2017) 304-309.
25. V. K. Joshi, P. Ram, R. K. Sharma and D. Tripathi, Porosity effect on the boundary layer Bodewadt flow of a magnetic nanofluid in the presence of geothermal viscosity, European Phys. J. Plus 132 (2017) Article ID:254.

26. M. Rahman and H. I. Andersson, On heat transfer in Bödewadt flow. Int J, Heat & Mass Transfer 112 (2017) 1057–1061.
27. T. Rafiq, M. Mustafa and M. Asif Farooq, Numerical assessment of Bödewadt flow and heat transfer over a permeable disk with variable fluid properties, Physica A 534 (2019) Article ID:122138.
28. T. Rafiq and M. M. Hashmi, Bödewadt flow over a permeable disk with -heterogeneous reactions: A numerical study, Appl. Sci. 9 (2019) Article ID:4046.
29. T. Rafiq, M. Mustafa and J. A. Khan, Numerical study of Bödewadt slip flow on a convectively heated porous disk in a nanofluid, Phys. Scr. 94 (2019) Article ID:095701.
30. M. Sheikholeslami, D.D. Ganji , M.M. Rashidi, Magnetic field effect on unsteady nanofluid flow and heat transfer using Buongiorno model, J. Magnet. & Magnet. Mater. 416 (2016) 164–173.
31. M. Turkyilmazoglu. Buongiorno model in a nanofluid filled asymmetric channel fulfilling zero net particle flux, Int. J. Heat & Mass Transfer 126 (2018) 974–979
32. D. Domairry, M. Sheikholeslami and H. R. Ashorynejad, Natural convection flow of a non-Newtonian nanofluid between two vertical flat plates, https://doi.org/10.1177/1740349911433468.
33. Arifin, N. A. Abu Bakar, N. Bachok, Rotating flow over a stretching sheet in nanofluid using Buongiorno model and thermophysical properties of nanoliquids, AIP Conference. Pros, 1870(1) (2017) Article ID:040017.
34. H. F. Oztop and E. Abu-Nada, Numerical study of natural convection in partially heated rectangular enclosures filled with nanofluids, Int. J. Heat Fluid Flow 29 (2008) 1326-1336.
35. S. P. Anjali Devi, T. Elakkiyapriya, Buongiorno model with revised boundary conditions for hydromagnetic forced convective nanofluid flow past a rotating porous disk, Int. J. Math. Trends & Tech. 55(3) (2018) 212-222.
36. Z. Haddad, E Abu Nada, H. F. Oztup and A. Mataoui, Natural convection in nanofluids: Are the thermophoresis and Brownian motion effects significant in nanofluid heat transfer enhancement?, Int J. Therm. Sci. 57 (2012) 152-162.
37. D. Wen and Y. Ding, Experimental investigation into convective heat transfer of nanofluids at the entrance region under laminar flow conditions, Int. J. Heat & Mass Transfer 47(24) (2004) 5181-5188.
38. M. A. Sheremet, E. Abu-Nada, M. S. Astanina, Combined effects of Thermophoresis, Brownian Motion, and nanofluid variable properties on CuO-Water nanofluid Natural

convection in a partially heated square cavity, Int J. Heat Transfer 140(8) (2018) Article ID:082401.

39. S. U. S. Jang, S.P. Choi, Role of Brownian motion in the enhanced thermal conductivity of nanofluids, Appl. Phys. Lett. 84 (2004) Article ID:4316.
40. E. Abu-Nada, Z. Masoud, H. F. Oztop and A. Campo, Effect of nanofluid variable properties on natural convection in enclosures, Int. J. Thermal. Sci. 49(3) (2010) 479-491.
41. K. Zaimi, A. Ishak and I. Pop, Unsteady flow due to a contracting cylinder in a nanofluid using Buongiorno's model, Int. J. Heat & Mass Transfer 68 (2014) 509-513.
42. M. A. Sheremet, E. Abu-Nada, M. S. Astanina, Combined effects of Thermophoresis, Brownian Motion, and nanofluid variable properties on CuO-Water nanofluid Natural convection in a partially heated square cavity, Int J. of Heat Transfer 140(8) (2018) Article ID:082401.
43. M. K. Nayak, A. K. Hakeem, O. D. Makinde, Time varying chemically reactive magneto-hydrodynamic non-Linear Falkner-Skan flow over a permeable stretching/shrinking wedge: Buongiorno model, J. Nanofluids 8 (2019) 467–476.
44. M. A. Sheremet, T. Gerosan and I. Pop, Natural convection in a wavy porous cavity with sinusoidal temperature distributions on both side walls filled with a nanofluid: Buongiorno's mathematical model, ASME J. Heat Transfer 137(7) (2015) Article ID:072601.
45. J. A. Khan, M. Mustafa, T. Hayat, M. Sheikholeslami and A. Alsaedi, Three-Dimensional flow of nanofluid induced by an exponentially stretching sheet: An application to solar energy, PLoS ONE 10(3) (2015), Article ID:0116603.
46. M. A. Sheremet, I. Pop and A Shenoy, Unsteady free convection in a porous open wavy cavity filled with a nanofluid using Buongiorno's mathematical model, Int. Commun. Heat Mass Transfer 67 (2015) 66–72.
47. R. K. Nayak, S. Bhattacharyya and I. Pop, Effects of nanoparticles dispersion on the mixed convection of a nanofluid in a skewed enclosure, Int. J. Heat & Mass Transfer 125 (2018) 908–919.
48. M. Sheikholeslami, D. D. Ganji and M. M. Rashidi, Magnetic field effect on unsteady nanofluid flow and heat transfer using Buongiorno model, J. of Magnetism & Magnetic Material 416 (2016) 164-173.

49. H. B. Rokni and M. Sheikholeslami, Effect of melting heat transfer on nanofluid flow in existence of magnetic field considering Buongiorno Model, Chinese J. Phys. 55(4) (2017) 1115-1126.
50. M. Mahmoodi, S. Kandelousi, Effects of thermophoresis and Brownian motion on nanofluid heat transfer and entropy generation, J. Mol. Liq. 211 (2015) 15-24.
51. M. Khan, A. Ahmed and J. Ahmed, Transient flow of magnetized Maxwell nanofluid: Buongiorno model perspective of Cattaneo-Christov theory, Applied Math. & Mech. (English Edition) 41(4) (2020) 655–666.
52. Z. A. S. Raizah, S. E. Ahmed, Convective transport in case of variable properties in porous enclosures with/without two heated ellipsis with rough boundaries, Alexandria Engg. J. (2020) https://doi.org/10.1016/j.aej.2020.06.048
53. H. Xu and M. D. K. Niazi, Modelling two-layer nanofluid flow in a micro-channel with electro-osmotic effects by means of Buongiorno's model, App. Math. & Mech. 41 (2020) 83–104.
54. A. Wakif, Z. Boulahia, S. R. Mishra, M. M. Rashidi and R. Sehaqui, Influence of a uniform transverse magnetic field on the thermo-hydrodynamic stability in water-based nanofluids with metallic nanoparticles using the generalized Buongiorno's mathematical model, Eur. Phys. J. Plus 133(181) (2018) https://doi.org/10.1140/epjp/i2018-12037-7
55. T. Von Kármán, Uber laminare und turbulente reibung, Z. Angew. Math. Mech. 1 (1921) 233–52.
56. M. Rahman and H. I. Andersson, Heat transfer in generalized vortex flow over a permeable surface, Int. J. Heat & Mass Transfer 118 (2018) 1090-1097.